WRF Model Sensitivity to Choice of Parameterization: A Study of the 'York Flood 1999'

Renji Remesan[1], Tim Bellerby[2], Ian Holman[1], Lynne Frostick[3]

[1] Cranfield Water Science Institute, Cranfield University

[2]Department of Geography, Environment and Earth Science, University of Hull

[3]Centre for Adaptive Science, University of Hull

Abstract:

Numerical weather modelling has gained considerable attention in the field of hydrology especially in un-gauged catchments and in conjunction with distributed models. As a consequence, the accuracy with which these models represent precipitation, sub-grid-scale processes and exceptional events has become of considerable concern to the hydrological community. This paper presents sensitivity analyses for the Weather Research Forecast (WRF) model with respect to the choice of physical parameterization schemes [both cumulus parameterisation (CPSs) and microphysics parameterization schemes (MPSs)] used to represent the '1999 York Flood' event, which occurred over North Yorkshire, UK, 1st -14th March 1999. The study assessed four CPSs [Kain–Fritsch (KF2); Betts–Miller–Janjic (BMJ); Grell–Devenyi ensemble (GD) and the old Kain–Fritsch (KF1)] and four MPSs [Kessler, Lin et al., WRF Single-Moment 3-class (WSM3) and WRF Single-Moment 5-class (WSM5)] with respect to their influence on modelled rainfall. The study suggests that the BMJ scheme may be a better cumulus parameterization choice for the study region, giving a consistently better performance than other three CPSs, though there are suggestions of underestimation. The WSM3 was identified as the best microphysics scheme and a combined WSM3/BMJ model setup produced realistic estimates of precipitation quantities for this exceptional flood event. This study analysed spatial variability in WRF performance through categorical indices including: POD, FBI, FAR and CSI during 'York Flood -1999' under various model settings. Moreover, the WRF model was good at predicting high intensity rare events over the Yorkshire region, suggesting it has potential for operational use.

Key words: numerical rainfall prediction; WRF, cumulus parameterization, microphysics York floods,

<u>Corresponding Address:</u>

Dr Renji Remesan

Cranfield Water Science Institute, Cranfield University

Vincent Building, Cranfield campus, MK43 0AL

E: r.remesan@cranfield.ac.uk

T: +44 (0)1234

1. Introduction:

Precipitation intensity, timing (onset timing and duration), spatial distribution of precipitation in basin etc. have great importance in state-of-art operational hydrology, integrated flood management approaches and advanced techniques to predict extreme hydrological events. Climate variability and its implications on water resources and extreme flood events have direct impacts on agriculture, road traffic, manufacturing and construction activities. Owing to climate change and its possible effects on water resources, hydrologists are seeking downscaling methods that can link atmospheric and hydrological models for hydrological simulations with reliable accuracy (Kite and Haberlandt., 1999; Wood et al., 2004). High-resolution global assimilated weather data from models such as the Weather Research and Forecasting (WRF) mesoscale model are very important sources of information capable of providing credible input data to modern regional hydrological models. Tang and Dennis (2014) evaluated the capability of WRF with the Variable Infiltration Capacity (VIC) hydrological model and highlighted good agreement in the simulation of monthly and daily soil moisture, and monthly evaporation in the Upper Mississippi River Basin (UMRB) from 1980 to 2010. This study highlighted that results from offline linkage of model could be used to reproduce certain climate variables and hydrological variables like soil moisture. Another reanalysis data driven WRF study by Wenhua and Chung-Hsiung (2013) reproduced the spatial distributions of daily mean precipitation and rainy days similar to that of Tropical Rainfall Measuring Mission (TRMM) Multisatellite Precipitation Analysis 3B42 product data in Western North Pacific. TRMM data are a widely acceptable global gridded data set among the hydrological community. Such WRF success stories in various environmental and geographic circumstances have accumulated knowledge and confidence in the hydrological community to directly use high resolution WRF outputs in their hydrological models (e.g. Liong et al 2013). In the meantime hydrologists are also interested in the sensitiveness in precipitation and other meteorological variables with WRF model structure. One can fine several studies of two-way coupling of the operational mesoscale weather prediction model with land surface hydrological models (Seuffert et al., 2002). Givati et al (2012) employed the WRF model to provide precipitation forecasts to run an operational streamflow forecast system for the Jordan River. Bugaets and Gonchukov (2014) have coupled WRF with Soil and Water Assessment Tool (SWAT 2012) using OpenMI 2.0 and web-service technologies and this integrated structure was used for real time hydrological modelling and forecasting

However, many publications have highlighted precipitation as one of the most difficult variables to simulate in numerical weather models and regional climate models (Giorgi et al., 1993; Zhang et al., 2003). A study by Pall and Eltahir (2001) has pointed out the difficulties of explicitly simulating local variability of atmospheric variables like precipitation rates at sub-grid scales in weather models. Therefore, many cumulus parameterization schemes (CPSs) and micro physical schemes have been developed and implemented in numerical weather prediction models to represent convective processes more effectively(e.g., Kuo 1974; Grell 1993). In a model, micro physical schemes mechanise processes controlling formation of cloud droplets and ice crystals, their growth and fallout as precipitation; whereas, the Cumulus convection plays a major role in the energetics and dynamics of atmospheric circulation systems (Kuo, 1974). Most of these schemes are developed in specific convective environments, so a systematic evaluation for the local climate of interest here is essential to yield useful information that can assist hydrological modellers who are specially working in catchment level (Ishak et. al., 2012). Seeing that many real-time floods forecasting and river level warning systems use high resolution data from mesoscale numerical models and couple these with state-of art- hydrological models, it is essential to assess the prediction sensitivity of the various meteorological variables obtained from various model configurations, scheme settings and diverse modelling resolutions. Many studies have identified that the selection of parameterization and microphysical schemes is the main reason for inconsistency of modelling and accuracy of predicted weather variables under various convective environments (Kerkhoven et al. 2006).

The WRF model is a next-generation mesoscale numerical weather prediction system designed in collaborative partnership, principally among the National Center for Atmospheric Research (NCAR) and the National Oceanic and Atmospheric Administration. It is one of the most sophisticated and widely accepted dynamic downscaling models in the literature for precipitation prediction. Fowle and Roebber (2003) and Fritsch and Carbone (2004) have highlighted the significance of cloud microphysics parameterizations in performance of the WRF model in rainfall modelling. Krishnamurti et al. (1999) suggested that there appears to be no single model that consistently gives best results, due not only to the chaotic nature of the atmosphere but also due to limitations in the initial conditions of the model and parameterisations. Ruiz and Saulo (2010) have used WRF over South America in different configurations to identify the best configuration which gives reliable estimates of observed surface variables. A number of sensitivity studies have considered the effects of different parameterization schemes including Cumulus Parameterization Schemes (CPSs) and microphysics parameterizations schemes (MPSs) (Hu et al 2010; Salimun et al 2010). Fovell and Su (2007) show how cloud microphysical parameterization and convection details significantly affect hurricane track forecasts at operational resolutions (30 and 12 km). They compared the effects of the Kessler, Lin et al, and the three class WRF single moment (WFR3) schemes, coupled with the effects of Kain-Fritsch (KF1), Grell-Devenyi (GD), and Betts-Miller-Janjic (BMJ) convective parameterization schemes.

This paper considers the evaluation and optimisation of different CPSs and MPSs of the WRF model with respect to the prediction of high intensity extreme events happening in the United Kingdom. The study focused on the Yorkshire Upper Derwent catchment located in the north east of England, which is consistently under flood risk. The Yorkshire Derwent Catchment Flood Management Plan (CFMP) has undertaken significant work to reduce the risk of flooding from the river especially following the March 1999 floods in the region. We will refer to this flood event as the York Flood – 1999. Reliable hydro-atmospheric conjunctive modelling systems play a significant role in the delivery of effective flood forecasting, flood warning and emergency response services during extreme high intensity precipitation events. The purpose of this study is to investigate the impact of WRF model settings in cumulus and microphysics parameterization schemes and to provide insight into the capabilities of modelling to reproduce rare storm events such as York flood - 1999. For this purpose, we have conducted high resolution WRF model simulations of the unprecedented rainfall events that occurred over the Yorkshire-Humber side region during first half of March-1999, using ECMWF ERA – 40 data as boundary conditions. We conducted rainfall simulations using several cumulus parameterization and microphysical schemes at different resolutions and compared the results with available ground based data. In this study, CPS sensitivity analysis was conducted using four schemes: Kain–Fritsch, KF2 (Kain 2004), Betts–Miller–Janjic, BMJ (Janjic 1994, 2000); Grell–Devenyi ensemble, GD (Grell and Devenyi 2002); old Kain–Fritsch, KF1 (Kain and Fritsch 1990). Four microphysics parameterization schemes (MPSs) were considered: Kessler (Kessler 1969); Lin et al. (Lin et al. 1983), WRF Single-Moment 3-class, WSM3 (Hong et.al. 2004); WRF Single-Moment 5-class, WSM5 (Hong et al., 2006). The study aimed to identify the best schemes and WRF model settings to represent individual transient rare weather systems for the Yorkshire-Humberside region and to reproduce the observed spatial variability and statistics of precipitation extremes.

In the subsequent sections of this paper, the land based observed precipitation data sets from the Yorkshire-Humberside region during York Flood -1999 and the WRF model setup are summarized. A detailed statistical analysis of the model performance under different settings of CPSs and MPSs against observations is presented in the results section. Finally, the discussions and conclusions are given in the fourth section of the paper.

2. Materials and Methods

2.1 Derwent and York Flood 1999

Yorkshire-Humberside region has a wide network of Rivers like Aire, Don, Esk (and coastal streams), Hull (and coastal streams), Ouse, Ribble and Tees alongside the River Derwent. The Yorkshire-Humber region is a winter flood prone part of England due to interactions of the major river network, significant storm rainfall in the catchments and substantial amount of snowmelt contributions to the rivers. This study focussed on the upper Derwent catchment extending over 1586 km^2, draining to Buttercrambe (UK Ordnance Survey Grid Reference SE 731587) in North Yorkshire. At the source and in the upper regions, the major river and its tributaries run over the Corallian limestone formation. The average annual rainfall in the region is 779 mm, out of which approximately 59% is accounted for by evapotranspiration. Annual rainfall over the northern half of the catchment (North York Moor) exceeds 1,000 mm in some years (Remesan, *et al.*, 2013).

The Derwent catchment has a long history of flooding with recorded evidence dating back to 1892. Prior to the heavy flooding in 1999, the previously highest recorded flood was in 1947 (Environment Agency, 2007). The catchment was particularly badly affected by flooding in 1927, 1930, 1931, 1932, 1947 and 1960 and in more recent times, during March 1999. In this study we are focusing on the capabilities of WRF to predict the rainfall which occurred during first two weeks of March which lead to the York flood - 1999. A low pressure fronts moved east to west between February 28th and March 9th, bringing first snow, then rain, so that melting snow added to the run-off. During 4-5th March 1999, exceptional levels of rainfall were experienced in the Derwent catchment area, reaching 125 millimetres (4.9 in) inside a 24 hour period. The situation was worsened by melting snow which had earlier accumulated on the North York Moors. Church Houses in Farndale had over 302 mm (11.89 inches) of rain between 28th February and 11th March, and other stations recorded similar figures (RNHS, 2013). In this study, simulated results obtained from WRF under different model settings were compared with observed data during 1st – 14th March of 1999 from 22 selected stations in the region. Details of those stations are given in the Table 1. The rainfall data observed at different points in the Derwent catchment are shown in Figure 2 and in a cumulative form in the Figure 3.

2.2 Weather Research and Forecasting (WRF) Model and Design of Experiments

The Advanced Research WRF version 3.3 (WRF, cited 2013) is a new-generation mesoscale modelling system (Skamarock et al., 2005) and successor of the well regarded MM5 model that serves both operational and research communities. WRF is a nonhydrostatic, primitive-equation, mesoscale meteorological model with advanced dynamics, physics and numerical schemes. The current WRF software framework (WSF) supports two dynamical solvers: the Advanced Research WRF (ARW) and the nonhydrostatic Mesoscale Model (NMM). These two solvers accompany a dynamic core which includes mostly advection, pressure-gradients, coriolis, buoyancy, filters, diffusion, and time-stepping. WRF possesses a number of outstanding features including: 1. Incorporation of advanced numerics and data assimilation techniques, 2. Multiple relocatable nesting capability, 3. Enhanced physics in treatment of convection and mesoscale precipitation, 4. Better handling of topography than the Eta model, 5. Much less diffusive, larger effective resolution, permits longer time steps. 6. Allows real data and idealized simulations in same framework, 7. Plug-in architecture, moving nests and nudging. These capabilities enable the model for a wide range of applications, from idealized research to operational forecasting, with priority given to horizontal grids of 1–10 kilometers. The WRF model uses terrain-following, hydrostatic-pressure vertical coordinates with the top of the model being a constant pressure surface. There are numerous physics options in the WRF model, the major details about its configuration in this study is shown in the Table 2. As shown in the Table 2, different physical parameterisations (e.g.: boundary layer, the convection and radiation schemes) including the Yonsei University scheme for the planetary boundary layer (Hong et al., 2006), the Dudhia shortwave radiation scheme (Dudhia, 1989), the rapid radiative transfer model for long-wave radiation scheme and Pleim-Xiu Land Surface Model have been used.

WRF is a mesoscale regional model that requires climatic data, generated by any global model, at its lateral boundaries to drive the model. In this study, the European Centre for Medium-Range Weather Forecasts (ECMWF), ERA-40 data set was used to drive it. Many sources of meteorological observations were used, including radiosondes, balloons, aircraft, buoys, satellites, and scatterometers over more than 40-years. The model initial and lateral boundary conditions are derived from the ECMWF 40-year reanalysis (ERA-40) data with the improved resolution of 1^0 x 1^0 and updated every 6 hour. The four nested domain dimensions of the WRF simulations for the Yorkshire-Humberside region are shown in Figure 1. The simulations of all selections of CPSs and MPSs were performed on a nested domain with the child domains [d02 (9 km), d03 (3km) and d04 (1km)] and parent domain [d01 (27 km)] as shown in figure 1. The four domains are centred over the Upper Derwent catchment with domain sizes of 918 x 756 km^2, 495 x 522 km^2, 246 x 255 km^2 and 103 x 94 km^2 for d04, d03, d02 and d01 respectively. Details of the grid spacing, grid number and the downscaling ratio of the experiments are given in Table 3. This study has performed simulations for each selection of CPSs and MPSs for 1176 hours (2 weeks) starting at 00.00 UTC 01st March 1999 and finishing at 00.00 UTC 15th March 1999. A total of 8 simulations were conducted using four different CPSs of the WRF model [KF1, KF2, BMJ and GD] and another four MPSs [Kessler, Lin et al scheme, WSM3 and WSM5]. Some details of different CPSs are given in Table 4. The resolution of the innermost domain was fixed with a horizontal grid spacing of 1 km. The time steps of the four domains, which also govern the time intervals of the output rainfall series, are set to 3 hrs, 1 hr, 1 hr and 1hr, respectively from the outermost to the innermost domain. However, here we have presented a comparison of daily temporal and spatial simulation results because of availability of good quality land based daily data from 22 weather stations.

2.3 Verification Methods for WRF Simulations

Both categorical and the continuous indices have been employed as statistical measures for the spatial and temporal verification of meteorological model outputs against land-based rainguage data (Stanski et al., 1989; Jolliffe and Stephenson, 2003; Wilks, 2006; Liu et al., 2012). The most commonly used categorical verification indices are the probability of detection (POD), frequency bias index (FBI), false alarm ratio (FAR) and the critical success index (CSI). The POD index gives an idea of the fraction of the observed precipitation that is correctly predicted by the model; this index ranges from 0 to 1, with 1 being a perfect score, and it is sensitive to the frequency of rainfall occurrence during the event. FBI gives an indication of overestimation or underestimation but it is also sensitive to how well precipitation simulations match observed values. The FBI ranges from 0 to ∞ with 1 indicating a perfect match. CSI ranges between 0 and 1 and this index specifies how the simulated precipitation corresponds to the observed precipitation. This index is a popular categorical verification index in numerical weather modelling. It is sensitive to 'hits' and penalises both 'misses' and 'false alarms' but does not distinguish sources of simulation error. FAR quantifies the fraction of the simulated rainfall that did not actually occur. This indictor ignores 'misses' and it is also sensitive to the frequency of precipitation occurrence during the event. The equations for these categorical indices are given below:

$$POD = \frac{1}{n}\sum_{1}^{n}\frac{PP_i}{PP_i + NP_i} \tag{1}$$

$$FBI = \frac{1}{n}\sum_{1}^{n}\frac{PP_i + PN_i}{PP_i + NP_i} \tag{2}$$

$$FAR = \frac{1}{n}\sum_{1}^{n}\frac{PN_i}{PP_i + PN_i} \tag{3}$$

$$CSI = \frac{1}{n}\sum_{1}^{n}\frac{PP_i}{PP_i + +PN_i + NP_i} \tag{4}$$

The above equations take values from a rain/no-rain contingency table relating modelled and observed precipitation. *PP* counts simulated precipitation/observed precipitation (hits) *PN* simulated precipitation/observed no precipitation (false alarms), *NP* simulated no precipitation /observed precipitation (misses) and *NN* simulated no precipitation / observed no precipitation (correct negatives). When comparing the spatial performance of the simulations, the results of the WRF model were compared with rain-gauge observations at each time step *i*, and then the values of the categorical indices at all the time steps are averaged. In the case of temporal comparisons, the indices are calculated using simulated and observed time series data at each rain gauge *i*, then averaged to yield a single index value for all rain gauges.

This study additionally employed the following continuous statistical indices: Nash–Sutcliffe model efficiency coefficient (NS), Correlation Coefficient (CORR), coefficient of determination (R^2), Slope (S), root mean square error (RMSE) and mean bias error (MBE) (see equations below).

$$NS = 1 - \frac{\sum_{i-1}^{n}\left[r_i(i) - p_i(i)\right]^2}{\sum_{i-1}^{n}\left[p_i(i) - \overline{p}_i\right]^2} \tag{5}$$

$$RMSE = \sqrt{\left(\frac{1}{n}\sum_{i-1}^{n}\left[r_i(i) - p_i(i)\right]^2\right)} \tag{6}$$

$$CORR = \frac{n\sum_{i-1}^{n}\left[r_i(i).p_i(i)\right] - \sum_{i-1}^{n}\left[r_i(i)\right]\sum_{i-1}^{n}\left[p_i(i)\right]}{\sqrt{n\sum_{i-1}^{n}\left[p_i(i)\right]^2 - \left(\sum_{i-1}^{n}\left[p_i(i)\right]\right)^2}.\sqrt{n\sum_{i-1}^{n}\left[r_i(i)\right]^2 - \left(\sum_{i-1}^{n}\left[r_i(i)\right]\right)^2}} \tag{7}$$

$$R^2 = \left(\frac{n\sum_{i-1}^{n}\left[r_i(i).p_i(i)\right] - \sum_{i-1}^{n}\left[r_i(i)\right]\sum_{i-1}^{n}\left[p_i(i)\right]}{\sqrt{n\sum_{i-1}^{n}\left[p_i(i)\right]^2 - \left(\sum_{i-1}^{n}\left[p_i(i)\right]\right)^2}.\sqrt{n\sum_{i-1}^{n}\left[r_i(i)\right]^2 - \left(\sum_{i-1}^{n}\left[r_i(i)\right]\right)^2}}\right)^2 \tag{8}$$

$$S = \frac{n\sum_{i-1}^{n}\left[r_i(i).p_i(i)\right] - \sum_{i-1}^{n}\left[r_i(i)\right]\sum_{i-1}^{n}\left[p_i(i)\right]}{n\sum_{i-1}^{n}\left[p_i(i)\right]^2 - \left(\sum_{i-1}^{n}\left[p_i(i)\right]\right)^2} \tag{9}$$

$$MBE = \frac{\sum_{i-1}^{n}\left[r_i - p_i\right]}{n} \tag{10}$$

Where n is the number of observations; r_i = simulated precipitation, p_i = simulated precipitation variables from WRF under particular parameterization scheme and $\overline{p}_i$ is mean observed precipitation. These indices can give an idea of spatial variation of WRF modelled results, comparing it with observed rainfall values from each weather station site. CORR value can give a measure of the strength and the direction of a linear relationship between observed and simulated precipitation time series. The coefficient of determination is useful as it gives a proportional measure of the variance of one variable that is predictable from another variable.

3. Results and Discussions

The performance of several CPSs and MPSs configurations of the WRF model was evaluated for the 'York flood- 1999' event precipitation covering 0000 UTC 01st March 1999 to 0000 UTC 15th March 1999. The main aim was to select the best parameterization design for operational weather prediction and climate downscaling over the region during exceptionally high precipitation. Both frontal and convective storms are common in the study area; the frontal storms normally produce precipitation over large areas, whereas convective storms produce precipitation over smaller areas. The daily precipitation values during the study period exhibited varying temporal trends, which are the stations, were spatially heterogeneous. The temporal and spatial variation of daily precipitation is shown in the Figure 4 as obtained by Krigging interpolation of daily values from 22 nearby stations in the Upper Derwent catchment. In this figure it is evident that there is considerably high precipitation on 4- 6th of March in the upper Derwent River catchment with value of 67.7 mm at DANBY MOOR CENTRE (54.46, -0.89) on 6th of March 1999. Similar high values were observed at KILDALE: EAST GREEN BECK (54.48 -1.04), SCALING RESR NO 3 (54.51 -0.84), RANDY MERE RESR (54.41 -0.75), IRTON P STA (54.24 -0.46) and RAVENSWICK (54.28 -0.92) with values of 40.2 mm/day, 48.2 mm/day, 47.8 mm/day, 40.2 mm/day and 42.5 mm/day respectively. The stations with higher values are predominantly in the northern part of the Derwent Basin. As explained earlier a four domain configuration setups were used in this study with the inner domain dimension of 103 x 94 km^2 [1 km resolution, downscaling ratio of 1:3 and modelling time step 1 hr.]. The WRF model with this set up downscaled the ERA-40 Reanalysis data for 14 days using different CPSs and MPSs scenarios. Apart from the identification of a useful model setup for the region, it is also important to evaluate variability in spatial and temporal distribution of these downscaled precipitation outcomes from the WRF. This is because these values could directly be applied to distributed hydrological models while WRF outcomes (areal average) could be directly used in lumped, semi-distributed and distributed hydrological models for flood forecasting and modelling. This section describes results of the sensitivity analyses of various CPSs [Kain–Fritsch (KF2) Betts–Miller–Janjic (BMJ), Grell–Devenyi ensemble (GD) and the old Kain–Fritsch (KF1)] and their spatial and temporal comparisons with 22 land based gauging stations. The corresponding temporal and spatial comparison results of MPSs [Kessler, Lin et al, WRF Single-Moment 3-class (WSM3) and WRF Single-Moment 5-class (WSM5)] using various categorical and the continuous indices are given below.

3.1 Spatial and Temporal Sensitivity of WRF to Cumulus Parameterization Schemes (CPS) Selection

The optimum cumulus parameterizations for precipitation are strongly dependent on the sub region (Mooney et al., 2013) of the study domain. Many studies have demonstrated the need to carefully select parameterization combinations when attempting to use WRF as a regional climate model especially when linked to regional hydrological models. In this study we have used WRF outputs from the 3rd domain for comparison with land based precipitation values. This is because in many studies it is assumed that the convective rainfall generation is explicitly resolved in the inner domain without cumulus parameterisation (Liu et al., 2012). The sensitivity analysis and variations in WRF simulation of the rainfall distribution in space and time are detailed in the Tables 5 and 6. The categorical indices (POD, FBI, FAR and CSI) together with the continuous indices (NS, R^2, R, RMSE, MBE and S) that are calculated for a 1 hour duration in both spatial and temporal dimensions are shown in these two tables. Statistically one can say that the best WRF model gives higher values of POD, CSI NS, and R^2 and lower values of FBI, FAR and continuous indices like RMSE and MBE. Table 5 shows the spatial variation of WRF simulations corresponding to the different CPS selections in the form of continuous indices [NS, R^2, R, RMSE, MBE and S (these are averaged values for the simulated 14 days period)] in comparison to the selected 22 weather stations. Whereas, Table 6 shows the temporal variations of WRF simulations corresponding to different CPS selection in the form of above mentioned continuous indices (spatially averaged). We have used several indices for this sensitivity analysis considering the chaotic nature of the convective environment. The chaotic nature of the atmosphere suggests that analyses of only one type of error (e.g. biases) are not sufficient to rate model forecasts and thus sensitivity analysis of different parameterizations, since errors in one variable may propagate to others and quickly degrade forecasts.

3.1.1 Spatial Comparison:

In this study we adopt a sensitivity analysis using the categorical indices for first instance and a second level verification employing continuous indices. The categorical indices can give a measure of the correctness of the model's precipitation occurrence or non-occurrence, but are less reliable when considering the quantity of precipitation thus not decisive in comparison to continuous indices in identifying the best CPSs/ MPSs. POD assesses what fraction of the actual rainfall events were detected by the model, and FAR gives the fraction of 'false alarms' in rainfall occurrences. Thus, in order to quantify the differences between precipitation produced by simulations with different CPSs the different categorical spatial statistics are calculated for the 'York Flood – 1999' period and are shown in Figure 5 along with corresponding values associated with changes of MPSs. The evaluations of these statistical indices provide information about the model's effectiveness in simulating a range of precipitation events. The catchment area average values of probability of detection (POD) and false alarm rate (FAR) are the major categorical indices, which range from 0.64–0.76 and 0.27–0.32, respectively. The highest values are associated with KF2 (POD= 0.69, FAR= 0.27) and the lowest are associated with GD (POD= 0.64, FAR= 0.29). An FBI values less than one implies under estimation in all four CPSs based simulations. From figure 5 one can note that, after spatial comparison of four CPSs based simulation results, the higher values of precipitation underestimation occurred for GD based simulations with lower values for BMJ based simulations. The higher CSI value is associated with KF1 based simulation but the numerical value of CSI of BMJ based simulation is very close with value of 0.65. Although it is difficult to reach a conclusion on the performance of different CPSs from the Figure 5, the lower average value of FAR and higher FBI, CSI and POD scores indicate better model performance for heavier precipitation events with the KF2 and BMJ cumulus schemes.

Table 5 summarizes the effect of different cumulus parameterizations on spatial estimates of precipitation. Considering the spatial variation of continuous indices for KF1-based simulations, it can be seen that overall poor performance of the model is associated with weather station IDs 19 and 20 (i.e. KELD HEAD and KIRBY MISPERTON) with low values of NS efficiency, R^2, R and negative values of Slope. These trends were similar in simulations with the other three CPSs (KF2, BMJ and GD). The weather station locations associated with poor performance are towards the middle of the River Derwent catchment. It is interesting to note that only these two stations have shown negative or near zero slope values in all four CPSs simulations with spatial comparison. This study also focused on continuous statistical indices (e.g. RMSE, NS) that include both systematic and non-systematic errors. This measure of total error might be more relevant to evaluating model performance and its ability to simulate atmospheric physics. An index like NS can give an assessment of the predictive power and efficiency of the WRF model as long as there is observed data to compare with the modelled results. If an NS value is less than zero, then the observed mean is a better predictor than the model. The NS value ranges between $-\infty$ to 1 and if model efficiency is close to 1, model reliability and accuracy will be close to the maximum. Out of 22 stations higher modelling efficiencies were associated with stations such as KILDALE: EAST GREEN BECK (ID = 4) and WHITBY COASTGUARD (ID=11) during KF1 and KF2 simulations. Both in BMJ and GD based simulations, KILDALE station exhibited higher efficiencies with values of 0.42 and 0.35 respectively. This station is one of those situated north of Derwent catchment which experienced high precipitation rates during the York Flood 1999 period. The bias and RMSE values didn't show any fixed pattern within the study area. Over the south east corner of the catchment ($54^{0}0'0''$ N - $54^{0}10'0''$ N to $0^{0}30'00''$W - $0^{0}40'00''$W), there is a strong positive bias in predicted WRF precipitation at all times of day and integration times. For a detailed comparison, the rainfall simulated by WRF with different CPSs is shown in Figure 6 for selected weather stations (along with different MPSs selection). Figure 6 shows daily averaged values of modelled precipitation during 1st -14th March 1999. One can clearly note from the Table 5, Table 6 and Figure 5 (a-d) that there is clear underestimation and overestimation within the basin corresponding to different weather station positions. Though there is overestimation in certain stations during certain time steps, the average value of MBE is always negative in all CPSs suggesting a high tendency towards underestimation. A comparison with a spatial average of the WRF precipitation output with that of observed output shows that BMJ scheme is superior to the other three when we consider indices like NS, R^2, R and Slope with values of -0.41, 0.38, 0.19 and 0.49 respectively. The Bias values were smaller in the case of the KF1 scheme with a value of -0.77 mm/day, which is closer to that of BMJ scheme. Though a bit higher, RMSE values of the BMJ scheme were closer to that KF2 scheme during spatial evaluation. In general one can say that the schemes have followed a performance trend of BMJ > KF1 > GD > KF2 during CPSs simulations. During these four simulations, the microphysics was fixed as WRF Single-Moment 5-class scheme. One can note from Figure 6 that BMJ modelled precipitation is largest in the majority of the weather stations, but KF1 over performed the BMJ cumulus scheme in stations like IRTON P STA, HOVINGHAM HALL, KELD HEAD and KIRBY MISPERTON when we considered daily average modelled precipitation during 'York Flood- 1999' period.

3.1.2 Temporal Comparison:

Figure 7 presents the temporal average skill scores for the 14 days studied during the 'York Flood -1999' based on different CPS simulations. The temporal spread of the CPS based predictions by WRF has been evaluated through statistical verification against the available land based observation datasets. The temporal average categorical indices have shown that all CPS members do well in terms of POD and FAR particularly during 4th -6th March 1999, but the scores of POD drop off rapidly towards the end of the simulation dates and false alarm ratios increased during those days. The numerical values of CSI are lower than those of spatial indices [the lower value is associated with GD value of 0.34]. The bias index has a similar tendency to that of the spatial comparisons but with a better value of 0.85 for the KF2 scheme. In the case of KF2 and BMJ the probability of detection values are almost same but the false alarm index is less in the case of KF2 scheme than the BMJ one. Considering all four categorical indices, one can say that the performance of cumulus schemes follow this pattern, KF2 > BMJ > KF1 > GD.

The NS values are negative for all four simulations which indicate that, this criterion is very sensitive to the quantification of systematic under-prediction errors. The simulated precipitation values from the model that included different CPSs schemes inadequately captured the measured rainfall responses in terms of low RMSE, high bias, lower regression coefficient and Nash efficiency index. The lower (better) MBE and NS indices were associated with the KF1 scheme. The continuous statistical values have shown better performance on 4th of March and poorer performance on 6th of March with high values of MBE and RMSE. It can be seen from the time averaged continuous statistical indices (excluding MBE), that the results of WRF model with KF2 are superior to that of other WRF models with CPSs. Although, it is difficult to reach a conclusion, it appears that the KF2 scheme performed better than the BMJ scheme (which was better during spatial comparison of CPSs) when making temporal comparisons. Apart from these statistical analyses, variations in cumulative precipitation during 1st -14th March 1999 as predicted by different CPSs in the study region were plotted and are given in Figure 8. This shows the higher capability of the BMJ and lower performance of GD schemes in this case study.

3.2 Spatial and Temporal Sensitivity of WRF to Microphysics parameterization schemes (MPS) Selection

State-of-art microphysical parameterization schemes are commonly used to predict precipitation distribution within convective systems and many studies have shown that these can make a considerable difference in the resultant simulation (Luo et al. 2010; Cohen and McCaul 2006). Thus, to assess impact of the parameterization of microphysical processes on the development of convective systems in Northern Yorkshire region during first two weeks of March -1999, we have performed simulations using four microphysics parameterizations with varying complexity as explained in previous sections. These simulation results were comprehensively compared in both spatial and temporal scales using traditional categorical verification statistics and continuous statistics to check the accuracy of precipitation forecasts. Four simulations of four MPSs were performed with identical configurations, except for differences in the cloud microphysics parameterizations. The BMJ scheme was used as it has proved to be the best cumulus scheme.

3.2.1 Spatial Comparison:

Figure 5 shows the spatial average categorical verification results for FBI, FAR, POD, and CSI in MPSs for the Upper River Derwent highlighted for the period 1st March -14th March. The categorical results in Figure 5 show that the changes in MPSs which are used to initialize the WRF model do not greatly affect the numerical values and fluctuating nature of the CSI. The highest CSI value was associated with WSM5 (0.62) and lowest with WSM3 (0.43). It is interesting to note that the categorical bias index value increased to 0.88 showing least bias for the WSM5 scheme based simulation in comparison to all other simulation scenarios. Over BIRDSALL HOUSE and HIGH MOWTHORPE station regions, both Kessler and the Lin et al scheme detect almost the same frequency of rain events during low rainfall periods and the bias index was above 0.95 showing low bias during that period. In the case of all four MPSs, both FBI and CSI have a similar trend to that of POD with slight disparity in the case of FAR. The combination of WSM5 and BMJ gave highest value of both POD and FBI; together with the lowest value of FAR. In the south east and north west corners of the basin (in positions like BIRDSALL HOUSE, HIGH MOWTHORPE, MONK END FARM, and KILDALE: EAST GREEN BECK) there are lower FAR scores in the case of all four MPSs scenarios. These results suggest that the best MPS selections based on categorical thresholds are WSM5 > Lin et. al. > WSM3 > Kessler for this study region.

The NS index, Correlation Coefficient, Coefficient of Regression and slope values all increased in the combination of BMJ scheme with WSM5, Lin.et al and WSM3 micro physics schemes. The best WRF model setting for a given strategy was selected in such a way that its performance is satisfactory with the selection of given CPSs and MPSs. This resulted in the spatial average of RMSE being reduced to 6.40 mm, 4.54 mm and 5.34 mm for MPS sections of Lin et al., WSM3 and WSM5 respectively. These values are an improvement of -30.20%, -50.49%, -41.76% over the combination with Kessler microphysics with KF1 cumulus scheme (Note: Kessler micro physics scheme was fixed when we e made comparative simulations for different CPSs in the earlier section). The MBE values have decreased by 28.78 %, 39.79 % and 51.98 % for the Lin et al; WSM3 and WSM5 micro physics schemes respectively. Considering both types of index the best model configuration for our study basin occurs when the WSM5 is combined with BMJ cumulus scheme. However, the performance of WSM3 combined with BMJ gives a similar value.

3.2.2 Temporal Comparison:

When categorical indices for whole simulation period are compared (Figure 7), POD results in both WSM5 and WSM3 microphysics are better but the highest value of the critical success index was associated with the Kessler scheme followed by WSM5 and WSM3. There was little difference in the bias index; however the WSM3 combination with BMJ was slightly better. The critical success index (CSI) is more stable and differs by only 2%-3% from the previous highest values. Statistical indicators show reasonably acceptable values for POD (0.69), FBI (0.88) and FAR (0.31), with a corresponding CSI value of 0.49, indicating a high level of success for the WSM3 in detecting rare events in this region. The corresponding values associated with WSM3 are 0.69, 0.88, 0.31 and 0.49, suggesting a comparable performance. The higher values of POD than that of FAR show the potential for WRF models to model convective precipitation in better way. However, in the case of the temporal comparison of Lin et. al. Scheme, the FAR value was shown to be slightly higher than POD.

In comparison to temporal values for CPSs schemes, better NS and MBE have been identified in both WSM3 and WSM5 micro physics schemes; but lower ones in Lin. et. al. scheme with NS values of -0.25, -0.25 and -1.85 respectively. On the other hand, the coefficient of regression and correlation coefficient values increased only in the case of the WSM3 scheme. So considering both categorical and continuous indices it is possible to say the better microphysics is found in WSM3 followed by WSM5 when used in conjunction with the BMJ cumulus scheme. The cumulative variation of precipitation simulated using different microphysics schemes are shown in the Figure 9 which shows clearly the better performance of WSM3 in conjunction with BMJ cumulus scheme. To get a better idea of the variation of the WRF simulated precipitation (WSM3 in conjunction with BMJ) during the simulation time period, total precipitations at various time scales are shown in the form of 2D maps in Figure 10.

In this study convective and stratiform precipitation with the BMJ scheme is in more agreement with the land based observations in comparison to the other Cumulus schemes during the simulation scheme. Similar convective parameterization schemes are identified in a recent WRF sensitivity analysis to downscale summer rainfall over South Africa (Ratna et al., 2014). The lowest track error of cyclones simulated in a recent study by Chandrasekar and Balaji (2012) with numerical experiments for different cumulus schemes were associated with the experiment with the BMJ scheme for a 24-hr forecast time. WSM3 usually generates the shallowest storm and slowest deepening rate (Li and Pu, 2008). The differences in performance of WSM3 and WSM4 depend on the inclusion and exclusion of mixed-phase microphysical processes and the method of representing melting-freezing processes. Li and Pu (2008) showed that WSM3 could predict type 1 hurricanes whereas the WSM5 produced a storm value 12 hPa deeper than that in WSM3. Evans et al (2012) suggests WSM3 is a simpler but robust scheme than other more complex schemes that include other classes (cloud water, cloud ice, rain,snow, vapour). The analysis of Evans et al (2012) of the overall bias reveals that the precipitation is sensitive to BMJ generally producing lower bias in comparison to other cumulus scheme. A recent study by Alam (2014) has shown better performance of WSM3 in heavy rainfall generation over Bangladesh. The study showed that the WSM3 and Kessler schemes coupling with KF1 and BMJ schemes simulated significant amounts of rain water mixing ratio between 500 and 100 hPa, but WSM3 simulated a much higher rain water mixing ratio than that of the Kessler scheme. But in general Lin–KF1 combination gave better performance in this region. It indicates that the performance of BMJ or WSM3 schemes based on scores cannot be generalised in the study region, and it varies with the event's physical processes.

4. Conclusions:

This study investigated the sensitivity of the WRF mesoscale numeric weather model to the selection of CPS and MPS to model the Yorkshire – Humberside region (Upper River Derwent) during the 'York flood -1999' event. This analysis of convection permitting simulations was aimed at increasing the understanding of the role of parameterized cloud microphysics and cumulus schemes in the simulation of rare events in Northern Yorkshire focusing on the land based data from the Upper Derwent catchment. The results were compared with land based precipitation data from 22 rain gauges scattered around region.

This analysis demonstrates that the WRF simulation is very sensitive to the parameterization of cumulus and microphysical processes. The study has clearly indicated that all CPSs and MPSs schemes underestimated in describing the average quantity of daily precipitation during the 'York Flood – 1999' in all experiments, though there were few overestimations at certain locations for specific time steps. While statistical analysis using categorical and continuous indices gave slightly different results, we selected the best model setup by considering the superior categorical temporal indices, high values of R, R^2, RMSE and lower values of MBE. In general, the BMJ scheme successfully simulated the spatial and temporal features of the York flood-1999 although it produced underestimations in both spatial and temporal scales. The GD cumulus schemes performed poorly with persistent location bias, and failed to simulate the relevant features in both temporal and spatial scales. The performance of KF2 and KF1 was comparable but both schemes gave results with higher values of negative bias. The spatial comparison results were surprising as the relatively simple KF1 value outperformed the more complex KF2 and GD schemes which would normally be expected to produce superior results.

Relatively poor verification results suggest that it is also important to consider the interactions between various model physical parameterizations in order to find better overall combinations. For this reason, the study tested different microphysics configuration, fixing the cumulus scheme to BMJ. As for the BMJ convective schemes in the earlier case, better values of continuous indices were observed in the case of the WSM3 microphysics scheme which has outperformed all other three microphysics schemes in both spatial and temporal scales. There was slight disparity in the case of values obtained from categorical indices. WSM5 had more favourable categorical index values than WSM3 during temporal comparison, whereas in the spatial comparison, the WSM3 has outperformed WSM5. Unlike all other combinations tested in the Derwent basin during the 'York Flood – 1999' period, the model setup employing a combination of WSM5 and BMJ schemes produced superior results over all the other seven model set-ups. This study has highlighted the influence of explicit moisture schemes and microphysics on rainfall intensity prediction using WRF.

Properly parameterized mesoscale numerical model outputs can provide inputs for spatially explicit distributed hydrologic models that use grid cells as a primary hydrologic unit. For example, integrated systems like WRF-Hydro can be successfully applied to any region considering atmospheric, land surface and hydrological processes on grid scale (Gochis et al., 2014). A study by Nicholas et al (2013) highlighted the use of mescoscale model meteorological data in stream flow and snowpack response modelling in significantly data limited mountainous region. WRF could also be integrated with urban modelling systems to tackle related issues and to bridge the gaps between mesoscle and microscale modelling (Chen et al., 2011). Fowler (2005) noted that Yorkshire floods are a product of complex interaction of the spatial-temporal rainfall pattern and hydrological connectivity of ungauged catchments. This study has presented a case study at a catchment scale focusing on flood events that occurred in a certain year. As it looked at a single event in detail the results may not be generalizable to all forms of convection occurring in Yorkshire-Humberside region. The primary contribution of this study is to provide some insight into how critical is the choice of cumulus and microphysics parameterization in regional scale. However it has highlighted how choice of parameterization can influence model results and has indicated how this can be very important in predicting high intensity rainfall events. Accurate prediction depends on horizontal/vertical resolutions, coupling with ocean, data assimilation, model initialization etc. The choice of the downscaling ratios also would have an influence of downscaled precipitation.

5. **Acknowledgements**

This study was funded by Yorkshire Forward within the research project ‘Low Carbon and Climate Resilient Regional Economy’ which has the objective of a assessing the impacts of climate change on resources that influence the future regional economy of the Yorkshire – Humberside region in North-East England.

6. **References**

Alam MM (2014) Impact of cloud microphysics and cumulus parameterization on simulation of heavy rainfall event during 7–9 October 2007 over Bangladesh. J. Earth Syst. Sci. 123, 2: 259–279

Bugaets A, Gonchukov L (2014) Application of WRF - SWAT OpenMI 2.0 based models integration for real time hydrological modelling and forecasting. Geophysical Research Abstracts. 16, EGU2014-4712

Chandrasekar R, Balaji C (2012). Sensitivity of tropical cyclone Jal simulations to physics parameterizations. J. Earth Syst. Sci. 121, 4: 923–946

Chen F, Kusaka H, Bornstein R, Ching J, Grimmond CSB, Grossman-Clarke S, Loridan T, Manning KW, Martilli A, Miao S, Sailor D, Salamanca FP, Taha H, Tewari M, Wang X, Wyszogrodzki AA, Zhang C (2011). The integrated WRF/urban modelling system:

Development, evaluation, and applications to urban environmental problems. Int. J. Climatol. 31: 273–288. DOI: 10.1002/joc.2158.

Cohen C, McCaul Jr EW (2006) The sensitivity of simulated convective storms to variations in prescribed single-moment microphysics parameters that describe particle distributions, sizes, and numbers. Mon. Wea. Rev. 134: 2547-2565.

Dudhia J (1989) Numerical study of convection observed during the winter monsoon experiment using a mesoscale two-dimensional model. Journal of the Atmospheric Sciences 46(20): 3077–3107.

Environment Agency (2007) Managing Flood risk. Yorkshire Derwent Catchment Flood Management Plan May 2007. www.knowledge-controversies.ouce.ox.ac.uk/Ryedale2/.../DCFMP.pdf (downloaded on 29/05/2013).

Evans JP, Ekstrom, M, Ji F. (2012). Evaluating the performance of a WRF physics ensemble over South-East Australia. Clim Dyn 39:1241–1258 DOI 10.1007/s00382-011-1244-5

Fovell RG, Su H (2007) Impact of cloud microphysics on hurricane track forecasts. Geophys. Res. Lett. 34, L24810.

Fowler MA, Roebber PJ (2003) Short-range (0-48 h) numerical prediction of convective occurrence, mode, and location. Weather and Forecasting 18: 782–794.

Fritsch JM, Carbone RE (2004) Improving quantitative precipitation forecasts in the warm season: a USWRP research and development strategy. Bulletin of the American Meteorological Society 85(7): 955–965.

Giorgi F, Bates GT, Nieman SJ. 1993. The multiyear surface climatology of a regional atmospheric model over the western United States. Journal of Climate 6: 75–95.

Givati A, Barry L, Yubao L, Alon R, (2012) Using the WRF Model in an Operational Streamflow Forecast System for the Jordan River. J. Appl. Meteor. Climatol, 51, 285–299 doi: http://dx.doi.org/10.1175/JAMC-D-11-082.1

Grell GA (1993) Prognostic evaluation of assumption used by cumulus parameterizations. Mon. Wea. Rev. 121: 764-787.

Grell GA, Devenyi D (2002) A generalized approach to parameterizing convection combining ensemble and data assimilation techniques. Geophys. Res. Lett. 29(14), 1-4. doi: 10.1029/2002GL015311.

Gochis D, Rasmussen R, Yu W, Ikeda, K (2014). Modeling changes in extreme snowfall events in the Central Rocky Mountains Region with the Fully-Coupled WRF-Hydro Modeling System. Geophysical Research Abstracts 16. EGU2014-16094

Hong SY, Dudhia J, Chen SH (2004) A Revised Approach to Ice Microphysical Processes for the Bulk Parameterization of Clouds and Precipitation. Mon. Wea. Rev. 132: 103–120.

Hong SY, Noh Y, Dudhia J (2006) A new vertical diffusion package with an explicit treatment of entrainment processes. Monthly Weather Review 134: 2318–2341.

Hu M, Nielsen-Gammon JW, Zhang F (2010) Evaluation of three planetary boundary layer schemes in the WRF model. J. Appl. Meteor. Climatol. 49: 1831–1844.

Ishak A, Bray M, Remesan R, Han D (2012) Seasonal Evaluation of Rainfall Estimation by four Cumulus Parameterization Schemes and their Sensitivity Analysis. Hydrological Processes. 26: 1062 – 1078. DOI: 10.1002/hyp.8194.

Janjic ZI (1994) The step-mountain eta coordinate model: Further developments of the convection, viscous sublayer and turbulence closure schemes. Mon. Weather Rev. 122: 927–945.

Janjic ZI (2000). Comments on "Development and evaluation of a convection scheme for use in climate models". J. Atmos. Sci. 57, 3686.

Jolliffe IT, Stephenson DB (2003) Forecast Verification: A Practitioner's Guide in Atmospheric Science. John Wiley and Sons: Chichester, UK; 240.

Kain JS (2004) The Kain–Fritsch convective parameterization: An update. J. Appl. Meteor. 43: 170–181.

Kain JS, Fritsch JM (1990) A one-dimensional entraining/detraining plume model and its application in convective parameterization. J. Atmos. Sci. 47(23): 2784–2802.

Kerkhoven E, Gan TY, Shiiba M, Reuter G, Tanaka K (2006) A comparison of cumulus parameterization schemes in a numerical weather prediction model for a monsoon rainfall event. Hydrol. Processes. 20: 1961–1978.

Kessler E (1969) On the distribution and continuity of water substance in atmospheric circula-tion. Meteor. Monogr. No. 32, Amer. Meteor. Soc., 84.

Kite GW, Haberlandt U (1999) Atmospheric model data for macroscale hydrology. Journal of Hydrology 217: 303–313. doi:10.1016/S0022-1694(98)00230-3.

Krishnamurti TN, Kishtawal CM, LaRow TE, Bachiochi DR, Zhang Z, and coauthors (1999) Improved weather and seasonal climate forecasts from multi-model superensemble. Science 285: 1548–1550.

Kuo HL (1974) Further studies of theparameterizations of the influence of cumulusconvection on large scale flow. J. Atmos. Sci. 31: 1232-1240

Li X, Pu, Z (2008). Sensitivity of Numerical Simulation of Early Rapid Intensification of Hurricane Emily (2005) to Cloud Microphysical and Planetary Boundary Layer Parameterizations. Monthly Weather Review 136. DOI: 10.1175/2008MWR2366.1

Lin YL, Farley RD, Orville HD (1983) Bulk parameterization of the snow field in a cloud model. J. Climate App. Meteor. 22: 1065-1092.

Liong SY, Raghavan SV, Vu MT (2013). Climate Change and Its Impacts on Streamflow: WRF and SCE-Optimized SWAT Models. Data Assimilation for Atmospheric, Oceanic and Hydrologic Applications (Vol. II). 411-428

Liu J, Bray M, Han D (2012) Sensitivity of the Weather Research and Forecasting (WRF) model to downscaling ratios and storm types in rainfall simulation. Hydrol. Process. 26: 3012–3031

Luo Y, Wang Y, Wang H, Zheng Y, Morrison H (2010) Modelling convective- stratiform precipitation processes on a Mei-Yu front with the Weather Research and Forecasting model: Comparison with observations and sensitivity to cloud microphysics parameterizations. J. Geophys. Res. 115: D18117.

Mooney PA, Mulligan FJ, Fealy R (2013) Evaluation of the Sensitivity of the Weather Research and Forecasting Model to Parameterization Schemes for Regional Climates of Europe over the Period 1990–95 J. Climate 26: 1002–1017. doi: http://dx.doi.org/10.1175/JCLI-D-11-00676.1.

Nicholas EW, Alan FH, Mimi H, Shara IF, Jessica DL (2013). Intercomparison of Meteorological Forcing Data from Empirical and Mesoscale Model Sources in the North Fork American River Basin in Northern Sierra Nevada, California. J. Hydrometeor. 14: 677–699. doi: http://dx.doi.org/10.1175/JHM-D-12-0102.1

Pall JS, Eltahir EAB (2001) Pathways relating soil moisture conditions to future summer rainfall within a model of the land-atmosphere system. J. Climate 14: 1227–1242.

Ratna SB, Ratnam JV, Behera SK, Rautenbach CJD, Ndarana T, Takahashi K, Yamagata T. (2014). Performance assessment of three convective parameterization schemes in WRF for downscaling summer rainfall over South Africa. Climate Dynamics 42,11-12: 2931-295310.1007/s00382-013-1918-2

Remesan R, Bellerby T, Frostick L (2013) Hydrological modelling using data from monthly GCMs in a regional catchment. Hydrol. Process. DOI: 10.1002/hyp.9872

Ruiz JJ, Saulo C (2010) WRF Model Sensitivity to Choice of Parameterization over South America: Validation against Surface Variables. Monthly Weather Review 138: 3342-3355.

Ryedale Natural History Society (RNHS) (2013) The March Floods. http://www.ryenats.org.uk/flood99.htm (downloaded on 23/05/2013).

Salimun E, Tangang F, Juneng L (2010) Simulation of heavy precipitation episode over eastern Peninsular Malaysia using MM5: Sensitivity to cumulus parameterization schemes. Meteorol. Atmos. Phys. 107: 33–49.

Seuffert G, Gross P, Simmer C, Wood EF (2002) The Influence of Hydrologic Modeling on the Predicted Local Weather: Two-Way Coupling of a Mesoscale Weather Prediction Model and a Land Surface Hydrologic Model. J. Hydrometeor 3, 505–523. doi: http://dx.doi.org/10.1175/1525-7541(2002)003<0505:TIOHMO>2.0.CO;2

Skamarock WC, Klemp JB, Dudhia J, Gill DO, Barker DM, Wang W, Powers JG (2005) A description of the Advanced Research WRF Version 2. NCAR Tech. Note/TN-468+STR, 88 pp.

Stanski HR, Wilson LJ, Burrows WR (1989) Survey of common verification methods in meteorology. World Weather Watch Technical Report No. 8, WMO/TD No.358, WMO, Geneva, 114.

Tang C, Dennis RL (2014) How reliable is the offline linkage of Weather Research & Forecasting Model (WRF) and Variable Infiltration Capacity (VIC) model?. Global and Planetary Change 116, 1–9.

Wenhua G, Chung-Hsiung S (2013) A Modeling Analysis of Rainfall and Water Cycle by the Cloud-resolving WRF Model over the Western North Pacific. Advances in Atmospheric Sciences. 30 (6) 1695–1711.

Wilks DS (2006) Statistical Methods in Atmospheric Science, 2nd Edn. Academic Press: Burlington, MA, 627.

Wood AW, Leung LR, Sridhar V, Lettenmaier DP (2004). Hydrologic implications of dynamical and statistical approaches to downscaling climate model outputs. Climatic Change 62: 189–216

WRF (2013) WRF model users page. http://www.mmm.ucar.edu/wrf/users/.

Zhang DL, Zheng WZ, Xue YK (2003) A numerical study of early summer regional climate and weather over LSA-East. Part I: model implementation and verification. Monthly Weather Review 131: 1895–1909.

Table Titles

Table 1: Details of different stations in Yorkshire –Humber region used for comparison of WRF results

Table 2: A brief summary WRF model configuration in Yorkshire-Humberside

Table 3: Details of nested domains, grid spacing and downscaling ratio used in Yorkshire-Humberside WRF modelling

Table 4: Comparison of the four WRF cumulus parameterization schemes used in this study

Table 5: Spatial comparison (in terms of different continuous statistical indices) of different CPSs based WRF results with corresponding weather stations

Table 6: Temporal comparison (in terms of different continuous statistical indices) of different CPSs based WRF results with corresponding weather stations

Figure Titles

Figure 1 Dimensions of the nested domains for different model settings which are centred over the River Derwent catchment, Yorkshire-Humberside. d01, d02, d03 and d04 refer to the four domains (NB: refer table 4 for details)

Figure 2: The observed rainfall during 1st March- 14th March 1999 from different stations at Derwent, Yorkshire [N.B. refer table 2 and figure 4 to for the locations of stations]

Figure 3: The accumulated rainfall during 1st March- 14th March 1999 from different stations at Derwent, Yorkshire [N.B. refer table 2 and figure 4 to for the locations of stations]

Figure 4: The spatial and temporal variation of precipitation during ‘York Flood – 1999’ period [N.B: the numbers are corresponding weather stations as mentioned in the table 2]

Figure 5: Spatial variation of categorical indices with selection of different CPSs and MPSs during York Flood – 1999

Figure 6: Scatter plots of the WRF simulated precipitation under different CPSs /MPSs and observed catchment precipitations during ‘York Flood -1999’ corresponding to different weather stations [N.B: 1:1 lines added to all figures]

Figure 7: Temporal variation of categorical indices with selection of different CPSs and MPSs during York Flood- 1999

Figure 8: Cumulative variation of WRF predicted precipitation during ‘York Flood – 1999’ using different CPSs

Figure 9: Cumulative variation of WRF predicted precipitation during ‘York Flood – 1999’ using different MPSs

Figure 10: The accumulated precipitation results obtained from WRF with WRF SM3 and BMJ schemes from 1st March to 14th march 1999

Table 1: Details of different stations in Yorkshire –Humber region used for comparison of WRF results

Number	Site	LAT	LONG
1	BIRDSALL HOUSE	54.076	-0.748
2	HIGH MOWTHORPE	54.105	-0.641
3	MONK END FARM	54.480	-0.963
4	KILDALE: EAST GREEN BECK	54.480	-1.043
5	CRATHORNE HOUSE	54.464	-1.322
6	SCALING RESR NO 3	54.505	-0.845
7	MULGRAVE CASTLE	54.501	-0.694
8	DANBY MOOR CENTRE)	54.466	-0.895
9	RANDY MERE RESR	54.409	-0.752
10	WHITBY	54.481	-0.624
11	WHITBY COASTGUARD	54.490	-0.604
12	SCARBOROUGH	54.273	-0.421
13	HIGH MOWTHORPE	54.105	-0.641
14	COXWOLD STORES	54.187	-1.182
15	IRTON P STA	54.242	-0.458
16	GANTON: GOLF CLUB	54.190	-0.494
17	RAVENSWICK	54.277	-0.916
18	HOVINGHAM HALL	54.173	-0.980
19	KELD HEAD	54.245	-0.806
20	KIRBY MISPERTON	54.198	-0.790
21	BIRDSALL HOUSE	54.076	-0.749
22	ELVINGTON W WKS	53.927	-0.927

Source: British Atmospheric Data Centre (badc.nerc.ac.uk)

Table 2: A brief summary WRF model configuration in Yorkshire-Humberside

Number	Features	Details
1	Nesting option	4 nests with 1 km inner and 27 km outer dimensions
2	Vertical coordinate	Terrain following σ_p
3	Horizontal grid	Arakawa-C
4	Projection	Lambert
5	Time integration scheme	Third-order Runga–Kutta scheme
6	Microphysics	Kessler scheme, Lin et.al. Scheme, WSM3, WSM5,
7	Convection	GD, BMJ, KF1, KF2
8	Radiation	Dudhia shortwave radiation scheme (Dudhia, 1989) and the rapid radiative transfer model long-wave radiation scheme (Mlawer et al., 1997)
9	Planetary boundary layer (PBL)	Yonsei University planetary scheme

10	Land surface model	Pleim-Xiu Land Surface Model (Xiu and Pleim, 2001)

Table 3: Details of nested domains, grid spacing and downscaling ratio used in Yorkshire-Humberside WRF modelling

Domain	**Time step (hour)**	**Grid (km)**	**Number of grids**	**Domain size (km2)**	**Downscaling ratio**
Domain 1	**3**	**27**	**34 x 28**	**918 x 756**	**-**
Domain 2	**1**	**9**	**55 x 58**	**495 x 522**	**1:3**
Domain 3	**1**	**3**	**82 x 85**	**246 x 255**	**1:3**
Domain 4	**1**	**1**	**103 x 94**	**103 x 94**	**1:3**

Table 4: Comparison of the four WRF cumulus parameterization schemes used in this study

CPSs	**Trigger function**	**Precipitation scheme**	**Closure assumption**	**Changes from predecessor and other details**
KF1	CAPE-based Cloud depth >4km	CAPE is removed from grid in convective	1D mass conservative cloud model	Nil

		time scale		No Shallow- convection No Momentum- tendencies Moisture tendencies: Qc Qr Qi Qs Cores: ARW
KF2	CAPE-based Cloud depth >3km	- Do -	- Do -	Cloud radius and cloud depth threshold for deep convection can vary The effects of shallow convection is also included No Momentum- tendencies Moisture tendencies: Qc Qr Qi Qs Cores: ARW

				NMM
BMJ	Based on an instability Cloud depth >200 hPa Sufficient moisture above cloud base	An adjustment towards an equilibrium reference profile	Adjustment scheme No cloud model	Reference profile and relaxation time depends on parameters that characterize the environment Trigger function to account for higher resolution No Momentum- tendencies Cores: ARW NMM
GD	Trigger function varies for each member but are commonly based on: CAPE CAPE trend Moisture convergence	Multi-closure, can be based on: CAPE Moisture convergence Low-level vertical velocity	Cloud model with updraft and downdraft fluxes No lateral entrainment and detrainment Changes in moisture is averaged over	Combines the strength of different closure assumptions in one scheme No Shallow- convection No Momentum- tendencies

			all members	Moisture tendencies: Qc Qi Cores: ARW NMM

Table 5: Spatial comparison (in terms of different continuous statistical indices) of different CPSs based WRF results with corresponding weather stations

CPSs	Indices	Weather station number																					
		1	**2**	**3**	**4**	**5**	**6**	**7**	**8**	**9**	**10**	**11**	**12**	**13**	**14**	**15**	**16**	**17**	**18**	**19**	**20**	**21**	**22**
KF1	**NS**	0.11	-0.05	0.03	0.44	0.25	0.20	0.26	-0.30	0.16	0.29	0.19	-1.43	-0.05	-0.57	-2.32	-0.70	-2.53	-0.21	-2.55	-0.85	0.11	0.25
	R2	0.35	0.25	0.20	0.73	0.55	0.62	0.59	0.68	0.69	0.60	0.50	0.28	0.25	0.26	0.26	0.28	0.16	0.22	-0.10	-0.06	0.35	0.52
	R	0.12	0.06	0.04	0.53	0.31	0.39	0.34	0.46	0.48	0.36	0.25	0.08	0.06	0.07	0.07	0.08	0.02	0.05	0.01	0.00	0.12	0.28
	MBE	0.73	0.42	8.54	-1.83	-0.41	-0.89	1.66	-7.02	-2.73	2.77	5.55	-1.75	0.42	-2.25	-3.92	-1.57	-6.76	-0.93	-6.17	-0.94	0.73	-0.55
	RMSE	6.32	6.55	16.96	12.22	6.16	11.56	8.82	16.60	9.97	9.59	10.17	8.71	6.55	5.14	11.94	6.52	15.52	5.30	15.22	7.36	6.32	4.12
	S	0.80	0.43	0.83	0.71	0.70	0.59	0.68	0.42	0.55	0.73	1.03	0.18	0.43	0.21	0.12	0.23	0.05	0.30	-0.04	-0.06	0.80	0.76
KF2	**NS**	0.19	-0.07	0.02	0.09	0.14	-0.10	-0.05	-0.59	-0.31	-0.21	0.29	-0.67	-0.07	-0.55	-1.60	-0.85	-2.54	-0.45	-2.24	-0.94	0.19	0.24
	R2	0.44	0.28	0.18	0.68	0.50	0.54	0.50	0.57	0.48	0.52	0.57	0.44	0.28	0.18	0.37	0.21	0.13	0.15	-0.05	0.03	0.44	0.50
	R	0.19	0.08	0.03	0.46	0.25	0.29	0.25	0.32	0.23	0.27	0.32	0.19	0.08	0.03	0.14	0.04	0.02	0.02	0.00	0.00	0.19	0.25
	MBE	0.25	0.18	6.17	-5.00	-1.30	-3.71	-1.48	-8.81	-4.02	-1.63	1.82	-1.94	0.18	-2.44	-4.24	-1.70	-6.90	-1.96	-6.89	-2.00	0.25	-0.08
	RMSE	5.34	5.87	14.13	13.21	6.40	12.82	8.70	18.95	12.94	8.43	6.32	8.04	5.87	5.62	11.56	6.80	15.70	5.18	15.19	6.55	5.34	4.63
	S	0.90	0.42	0.65	0.53	0.61	0.46	0.48	0.34	0.39	0.42	0.86	0.31	0.42	0.16	0.19	0.17	0.04	0.16	-0.02	0.03	0.90	0.83
BMJ	**NS**	0.15	0.00	0.03	0.42	0.27	0.21	0.30	-0.20	0.07	0.31	0.13	-1.33	0.00	-0.53	-2.27	-0.81	-2.63	-0.24	-2.39	-0.81	0.15	0.26

	R2	0.40	0.29	0.19	0.73	0.57	0.61	0.61	0.68	0.64	0.62	0.42	0.41	0.29	0.28	0.28	0.22	0.12	0.23	-0.08	0.00	0.40	0.52
	R	0.16	0.08	0.04	0.53	0.32	0.37	0.37	0.46	0.41	0.38	0.17	0.17	0.08	0.08	0.08	0.05	0.01	0.05	0.01	0.00	0.16	0.27
	MBE	1.02	0.95	8.51	-2.33	-0.45	-1.12	0.79	-7.08	-2.86	1.74	4.42	-2.55	0.95	-2.40	-4.24	-1.46	-6.65	-1.29	-6.57	-1.53	1.02	-0.32
	RMSE	6.32	6.60	17.05	12.23	5.97	11.98	8.44	16.54	10.75	8.78	9.58	8.08	6.60	5.12	11.94	6.76	15.63	5.14	15.25	7.03	6.32	4.28
	S	0.94	0.50	0.80	0.70	0.71	0.60	0.70	0.44	0.53	0.71	0.80	0.23	0.50	0.23	0.12	0.18	0.04	0.29	-0.03	0.00	0.94	0.80
GD	**NS**	0.08	-0.03	0.03	0.35	0.25	0.13	0.31	-0.33	0.01	0.31	0.19	-1.19	-0.03	-0.68	-1.91	-0.84	-2.54	-0.41	-2.33	-0.90	0.19	0.24
	R2	0.31	0.27	0.21	0.69	0.55	0.58	0.61	0.64	0.63	0.61	0.48	0.36	0.27	0.21	0.34	0.21	0.12	0.18	-0.06	0.07	0.44	0.50
	R	0.10	0.07	0.04	0.48	0.31	0.33	0.37	0.41	0.40	0.37	0.23	0.13	0.07	0.04	0.11	0.04	0.02	0.03	0.00	0.00	0.19	0.25
	MBE	0.39	0.25	8.78	-1.95	-0.46	-0.47	0.95	-6.50	-2.85	2.04	4.95	-1.96	0.25	-2.43	-4.22	-1.66	-6.85	-1.88	-6.75	-1.88	0.29	0.01
	RMSE	6.58	6.67	16.99	12.81	6.18	12.40	8.52	16.97	10.76	9.15	9.86	8.33	6.67	5.25	11.67	6.82	15.70	5.05	15.13	6.42	5.38	4.68
	S	0.74	0.46	0.85	0.66	0.71	0.56	0.71	0.41	0.50	0.73	0.98	0.23	0.46	0.17	0.16	0.17	0.04	0.20	-0.02	0.06	0.91	0.83

Table 6: Temporal comparison (in terms of different continuous statistical indices) of different CPSs based WRF results with corresponding weather stations

CPSs	Indices	**WRF Simulation days**													
		1-Mar-99	**2-Mar-99**	**3-Mar-99**	**4-Mar-99**	**5-Mar-99**	**6-Mar-99**	**7-Mar-99**	**8-Mar-99**	**9-Mar-99**	**10-Mar-99**	**11-Mar-99**	**12-Mar-99**	**13-Mar-99**	**14-Mar-99**
KF1	**NS**	-0.50	0.02	-0.17	0.28	0.02	-0.52	0.18	-1.21	0.02	-0.75	-0.13	-0.44	0.02	-0.07

	R2	0.09	0.57	0.46	0.69	0.51	0.49	0.51	0.66	0.33	0.33	0.08	0.54	0.30	0.10
	R	0.01	0.32	0.21	0.48	0.26	0.24	0.26	0.44	0.11	0.11	0.01	0.29	0.09	0.01
	MBE	-9.10	12.75	-3.02	5.43	-4.99	-14.57	9.57	-6.58	4.56	-3.68	0.00	-2.83	1.60	0.07
	RMSE	11.22	13.38	3.58	7.19	14.28	20.47	15.74	11.19	6.58	5.13	0.31	3.44	2.27	0.13
	S	0.01	2.33	0.30	1.01	0.51	0.24	0.92	0.22	0.57	0.11	0.18	0.10	0.59	0.22
KF2	**NS**	-0.51	0.03	-0.26	0.35	-0.07	-0.67	0.29	-1.32	0.22	-0.57	-0.24	-0.44	0.02	-3.05
	R2	0.04	0.69	-0.13	0.76	0.54	0.37	0.61	0.71	0.71	0.42	0.13	0.59	0.30	-0.08
	R	0.00	0.48	0.02	0.58	0.29	0.14	0.37	0.50	0.51	0.18	0.02	0.35	0.09	0.01
	MBE	-9.17	11.95	-3.10	4.73	-6.56	-17.99	6.64	-7.33	-1.70	-4.62	-0.04	-3.02	1.43	0.00
	RMSE	11.29	12.32	5.78	6.09	13.67	23.73	11.85	11.89	2.64	5.84	0.23	3.63	2.08	0.05
	S	0.00	2.28	-0.25	1.00	0.47	0.08	0.94	0.17	0.63	0.06	0.20	0.06	0.56	-0.05
BMJ	**NS**	-0.50	0.02	-0.52	0.32	0.07	-0.52	0.18	-1.30	0.20	-0.71	-0.14	-0.46	-0.17	-0.16
	R2	0.09	0.57	-0.07	0.72	0.53	0.46	0.51	0.65	0.55	0.33	0.13	0.39	0.08	0.08
	R	0.01	0.33	0.00	0.52	0.28	0.21	0.26	0.43	0.30	0.11	0.02	0.15	0.01	0.01
	MBE	-9.10	12.69	-1.38	5.23	-5.05	-15.19	9.55	-6.54	2.23	-4.07	-0.01	-2.92	0.89	0.04
	RMSE	11.22	13.26	3.96	6.93	13.92	21.11	15.79	11.26	3.97	5.44	0.27	3.55	1.82	0.10
	S	0.01	2.24	-0.09	1.06	0.54	0.22	0.91	0.21	0.75	0.07	0.25	0.06	0.14	0.14

GD	**NS**	-0.50	0.02	-0.10	0.30	0.05	-0.59	0.19	-1.34	0.18	-0.73	-0.11	-0.46	0.02	-0.50
	R2	0.06	0.54	0.19	0.71	0.54	0.46	0.52	0.67	0.47	0.40	0.12	0.36	0.35	-0.09
	R	0.00	0.29	0.03	0.50	0.29	0.22	0.27	0.45	0.22	0.16	0.01	0.13	0.12	0.01
	MBE	-9.17	12.95	-3.18	5.48	-5.46	-14.92	9.26	-6.30	3.33	-3.81	-0.01	-2.93	0.77	0.03
	RMSE	11.29	13.51	4.70	7.19	13.76	20.88	15.67	11.06	7.01	5.18	0.30	3.56	1.47	0.09
	S	0.01	2.11	0.28	1.04	0.53	0.20	0.95	0.21	1.18	0.10	0.25	0.06	0.52	-0.12

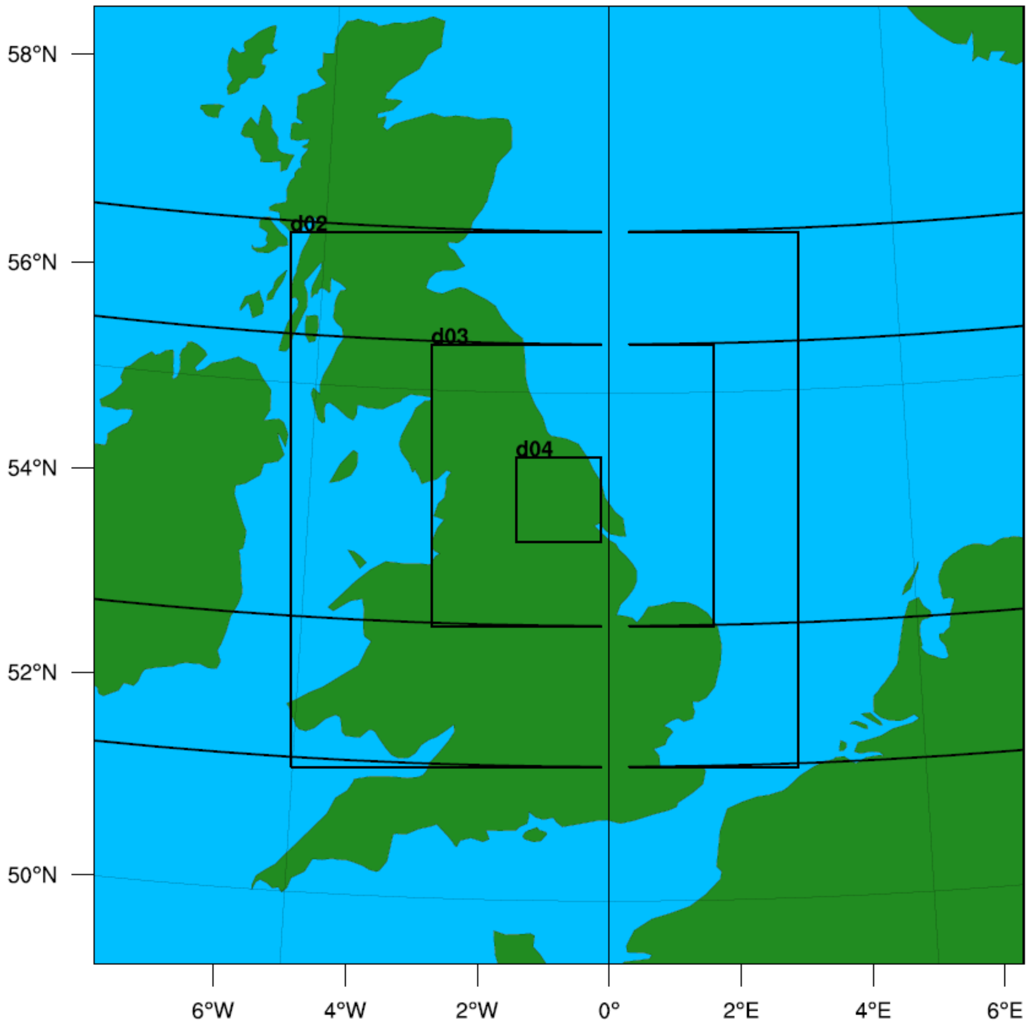

58°N
56°N
54°N
52°N
50°N
6°W
4°W
2°W
0°
2°E
4°E
6°E
d02
d03
d04

Figure 1 Dimensions of the nested domains for different model settings which are centred over the River Derwent catchment, Yorkshire-Humberside. d01, d02, d03 and d04 refer to the four domains (refer table 4 for details)

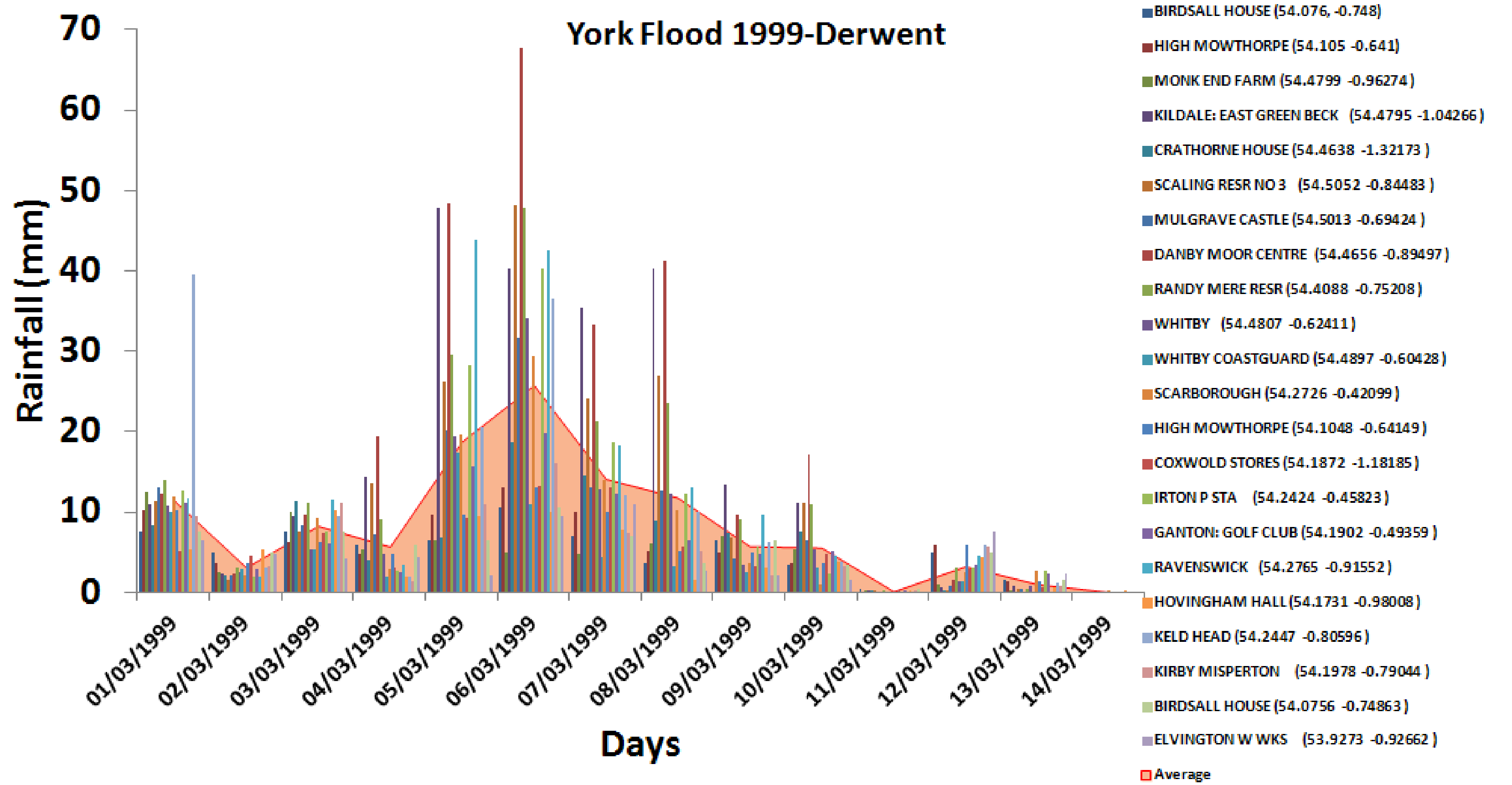

Figure 2: The observed rainfall during 1st March- 14th March 1999 from different stations at Derwent, Yorkshire [N.B. refer table 2 and figure 4 to for the locations of stations]

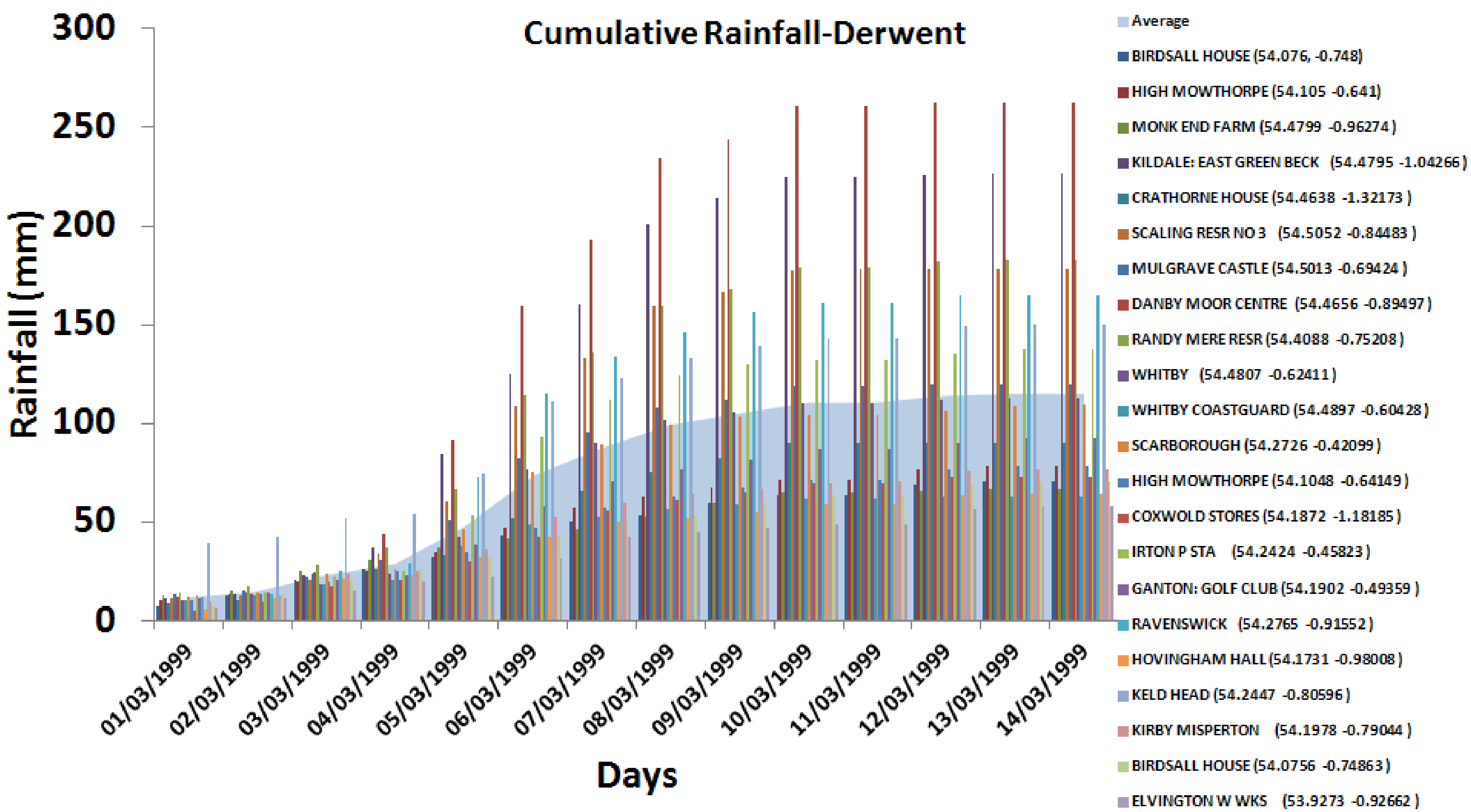

Figure 3: The accumulated rainfall during 1st March- 14th March 1999 from different stations at Derwent, Yorkshire [N.B. refer table 2 and figure 4 to for the locations of stations]

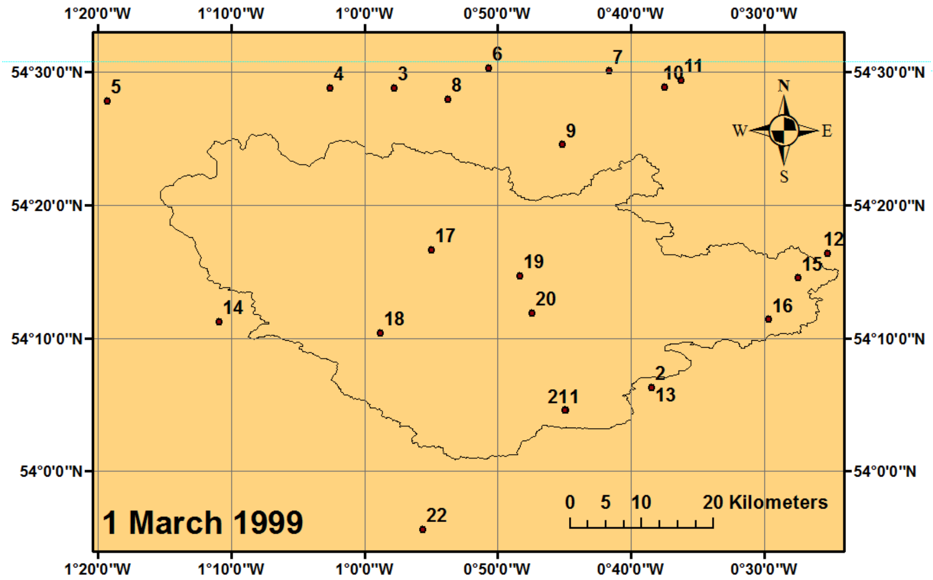
1 March 1999
1°20'0"W
1°10'0"W
1°0'0"W
0°50'0"W
0°40'0"W
0°30'0"W
54°30'0"N
54°20'0"N
54°10'0"N
54°0'0"N
N
S
W
E
0 5 10 20 Kilometers
1
2
3
4
5
6
7
8
9
10
11
12
13
14
15
16
17
18
19
20
21
22

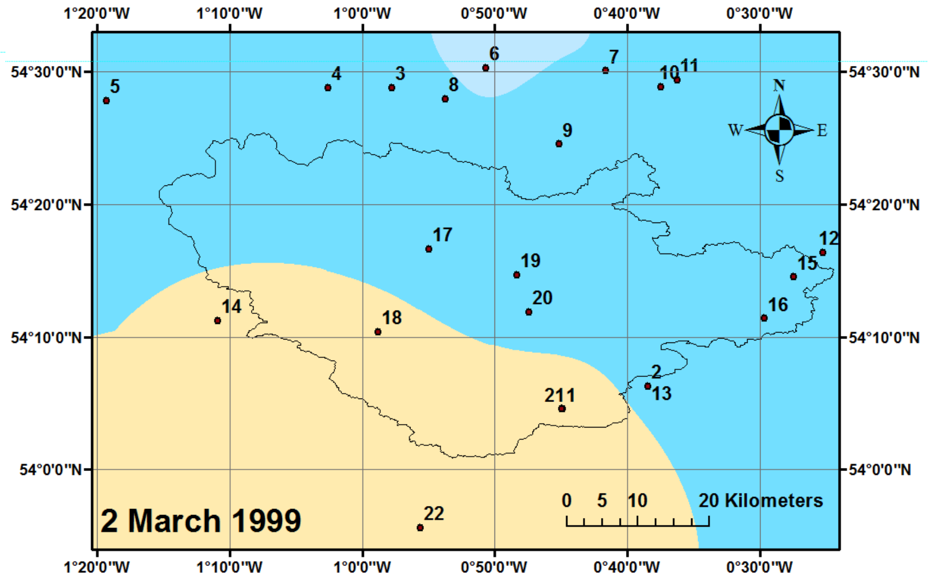
2 March 1999
1°20'0"W
1°10'0"W
1°0'0"W
0°50'0"W
0°40'0"W
0°30'0"W
54°30'0"N
54°20'0"N
54°10'0"N
54°0'0"N
N
S
W
E
0 5 10 20 Kilometers
1
2
3
4
5
6
7
8
9
10
11
12
13
14
15
16
17
18
19
20
21
22

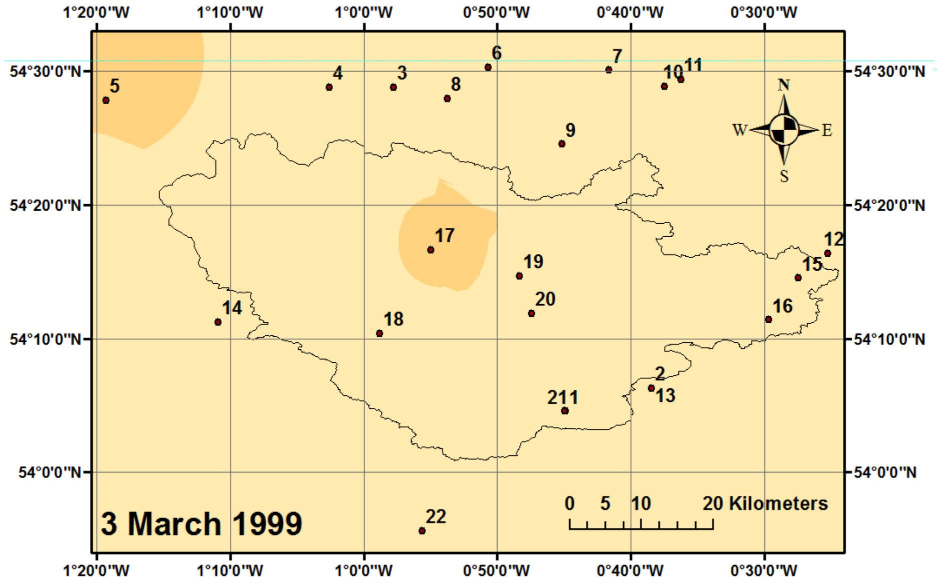
3 March 1999
20 Kilometers

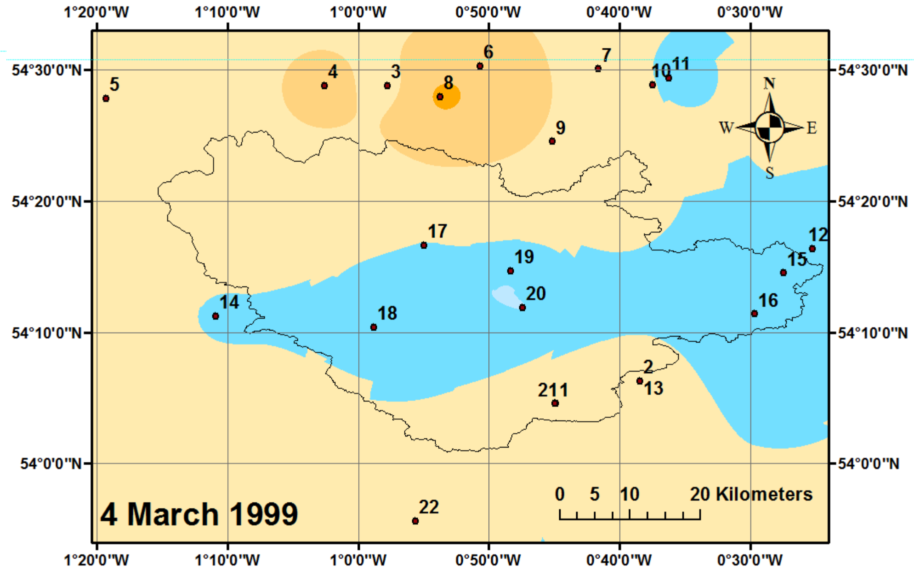
4 March 1999
20 Kilometers

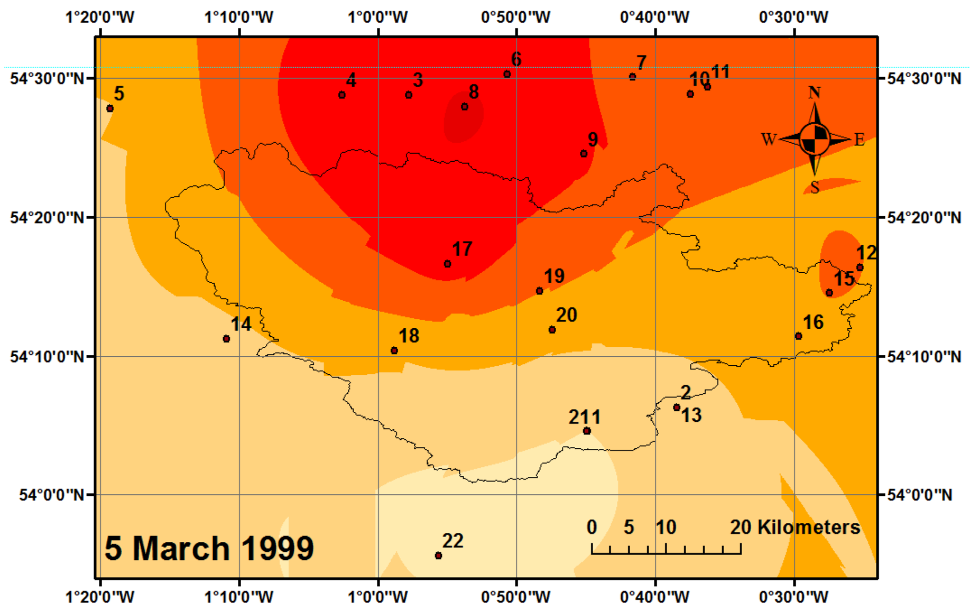

5 March 1999
1°20'0"W
1°10'0"W
1°0'0"W
0°50'0"W
0°40'0"W
0°30'0"W
54°30'0"N
54°20'0"N
54°10'0"N
54°0'0"N
0 5 10 20 Kilometers
N
S
W
E

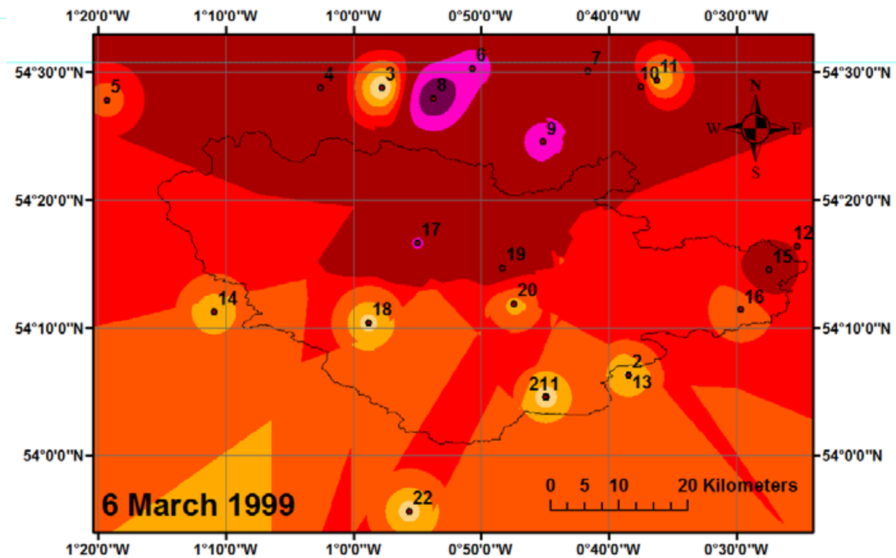

6 March 1999
1°20'0"W
1°10'0"W
1°0'0"W
0°50'0"W
0°40'0"W
0°30'0"W
54°30'0"N
54°20'0"N
54°10'0"N
54°0'0"N
0 5 10 20 Kilometers
N
S
W
E

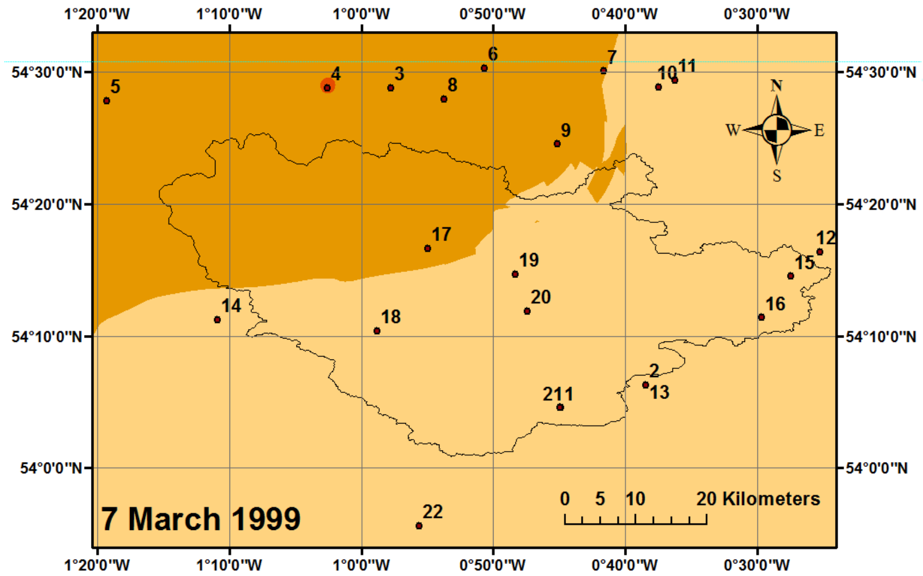
1°20'0"W
1°10'0"W
1°0'0"W
0°50'0"W
0°40'0"W
0°30'0"W
54°30'0"N
54°20'0"N
54°10'0"N
54°0'0"N
N
S
W
E
5
4
3
8
6
7
10
11
9
17
19
20
12
15
16
14
18
2
13
211
22
0 5 10 20 Kilometers
7 March 1999

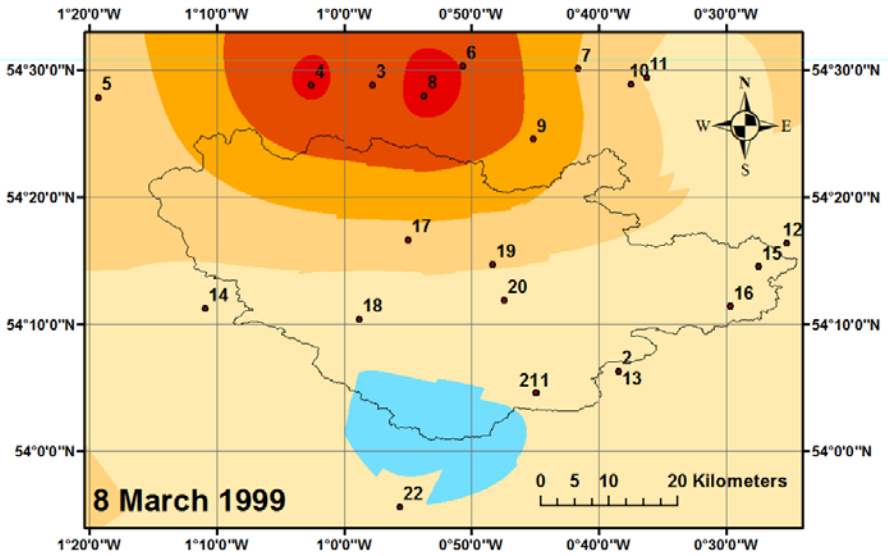
1°20'0"W
1°10'0"W
1°0'0"W
0°50'0"W
0°40'0"W
0°30'0"W
54°30'0"N
54°20'0"N
54°10'0"N
54°0'0"N
N
S
W
E
5
4
3
8
6
7
10
11
9
17
19
20
12
15
16
14
18
2
13
211
22
0 5 10 20 Kilometers
8 March 1999

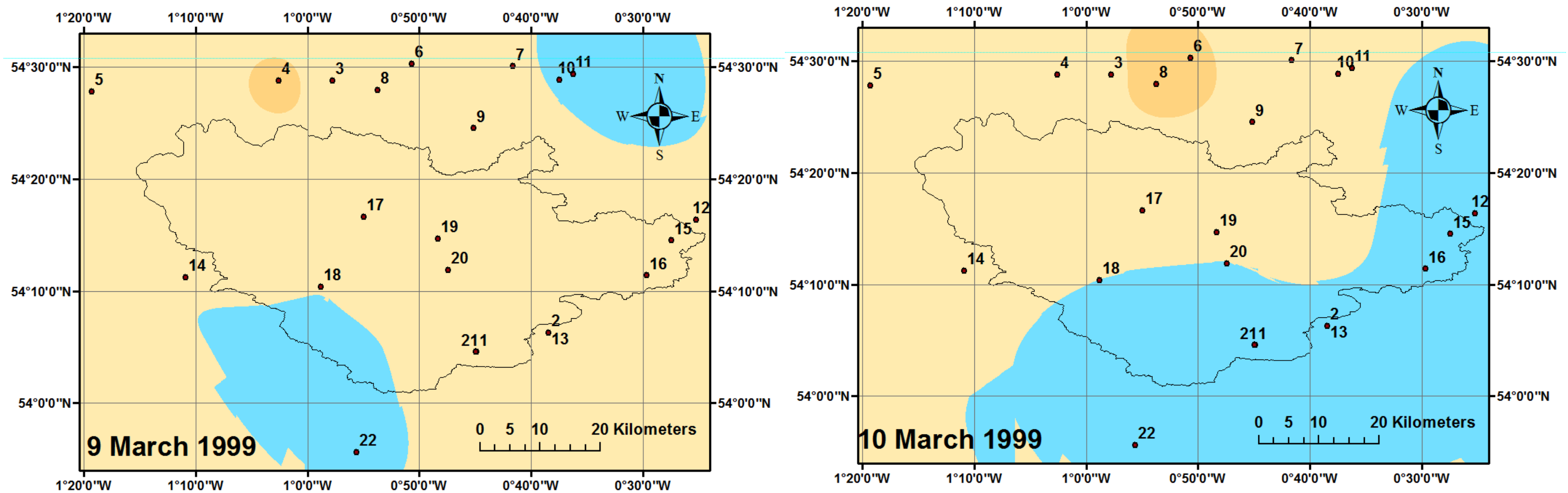
1°20'0"W
1°10'0"W
1°0'0"W
0°50'0"W
0°40'0"W
0°30'0"W
54°30'0"N
54°20'0"N
54°10'0"N
54°0'0"N
N
S
W
E
0
5
10
20 Kilometers
9 March 1999
10 March 1999
1
2
3
4
5
6
7
8
9
10
11
12
13
14
15
16
17
18
19
20
21
22

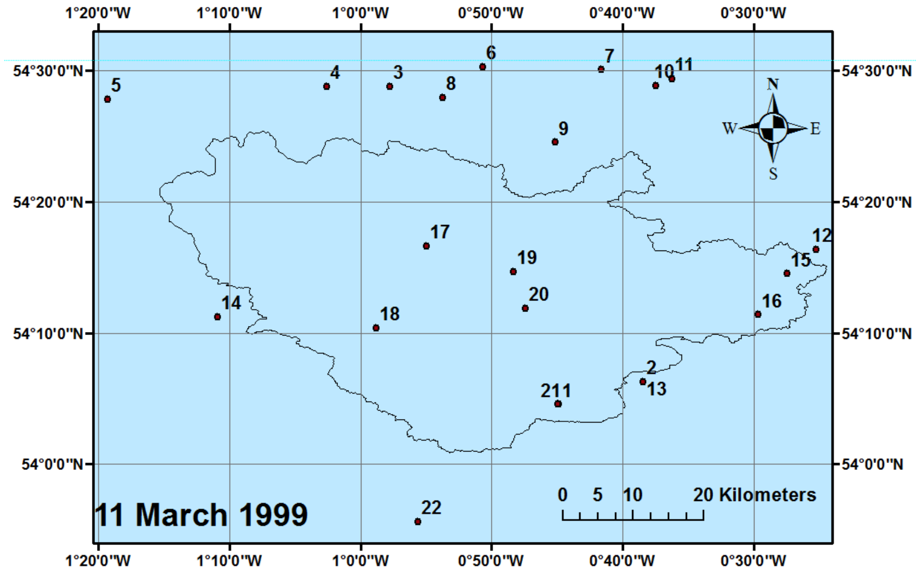
1°20'0"W
1°10'0"W
1°0'0"W
0°50'0"W
0°40'0"W
0°30'0"W
54°30'0"N
54°20'0"N
54°10'0"N
54°0'0"N
N
S
W
E
0 5 10 20 Kilometers
11 March 1999

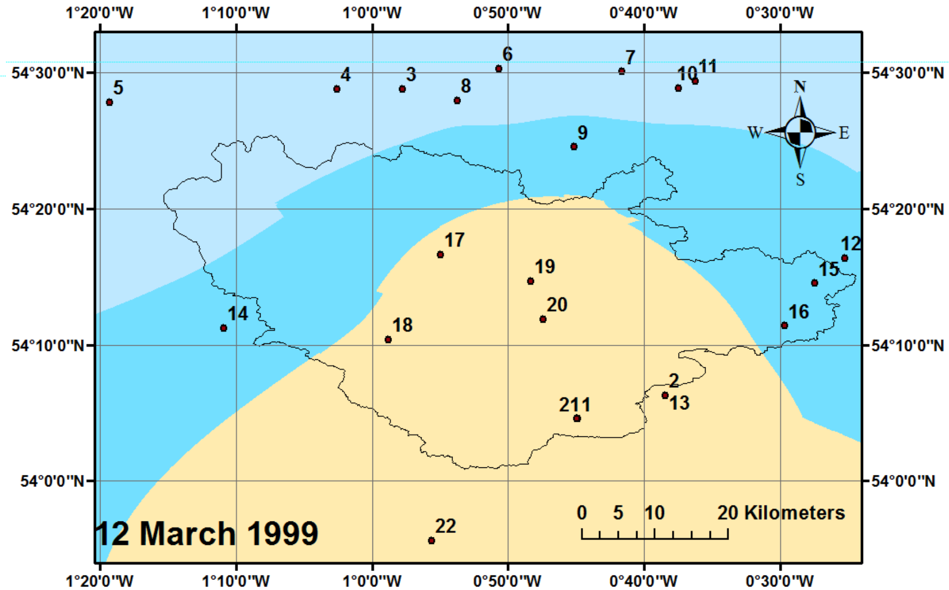
1°20'0"W
1°10'0"W
1°0'0"W
0°50'0"W
0°40'0"W
0°30'0"W
54°30'0"N
54°20'0"N
54°10'0"N
54°0'0"N
N
S
W
E
0 5 10 20 Kilometers
12 March 1999

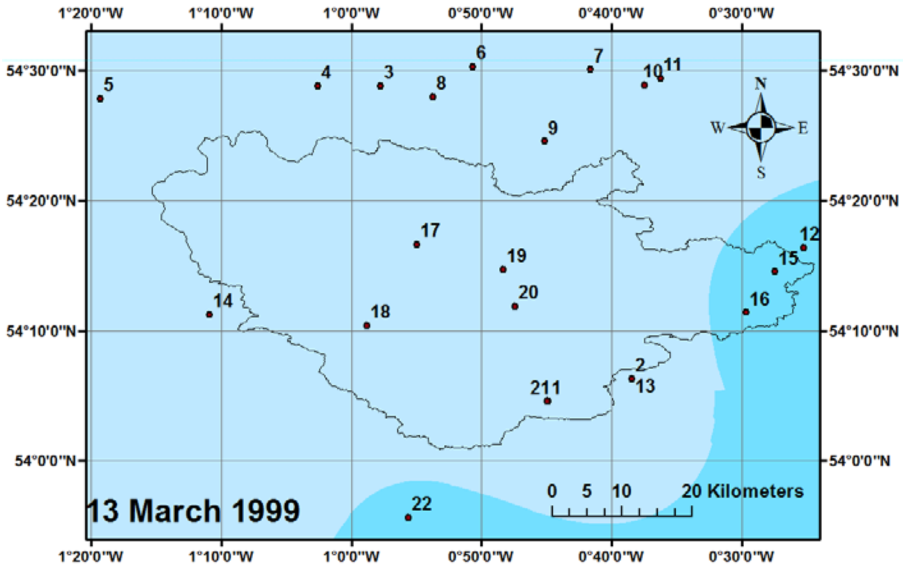
13 March 1999
0 5 10 20 Kilometers
1°20'0"W
1°10'0"W
1°0'0"W
0°50'0"W
0°40'0"W
0°30'0"W
54°30'0"N
54°20'0"N
54°10'0"N
54°0'0"N
N
S
W
E

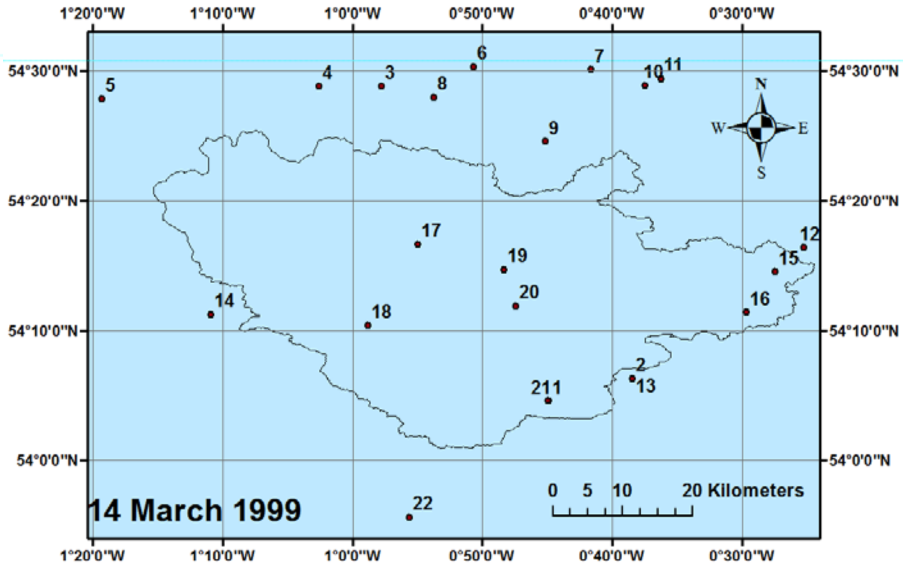
14 March 1999
0 5 10 20 Kilometers
1°20'0"W
1°10'0"W
1°0'0"W
0°50'0"W
0°40'0"W
0°30'0"W
54°30'0"N
54°20'0"N
54°10'0"N
54°0'0"N
N
S
W
E

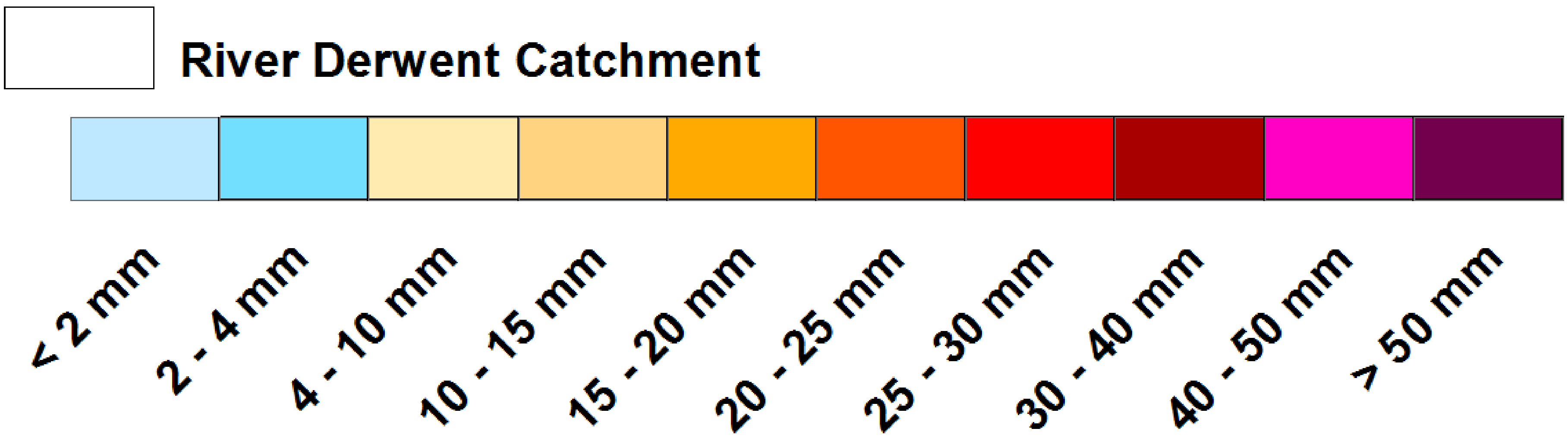

Figure 4: The spatial and temporal variation of precipitation during 'York Flood – 1999' period [N.B: the numbers are corresponding weather stations as mentioned in the table 2]

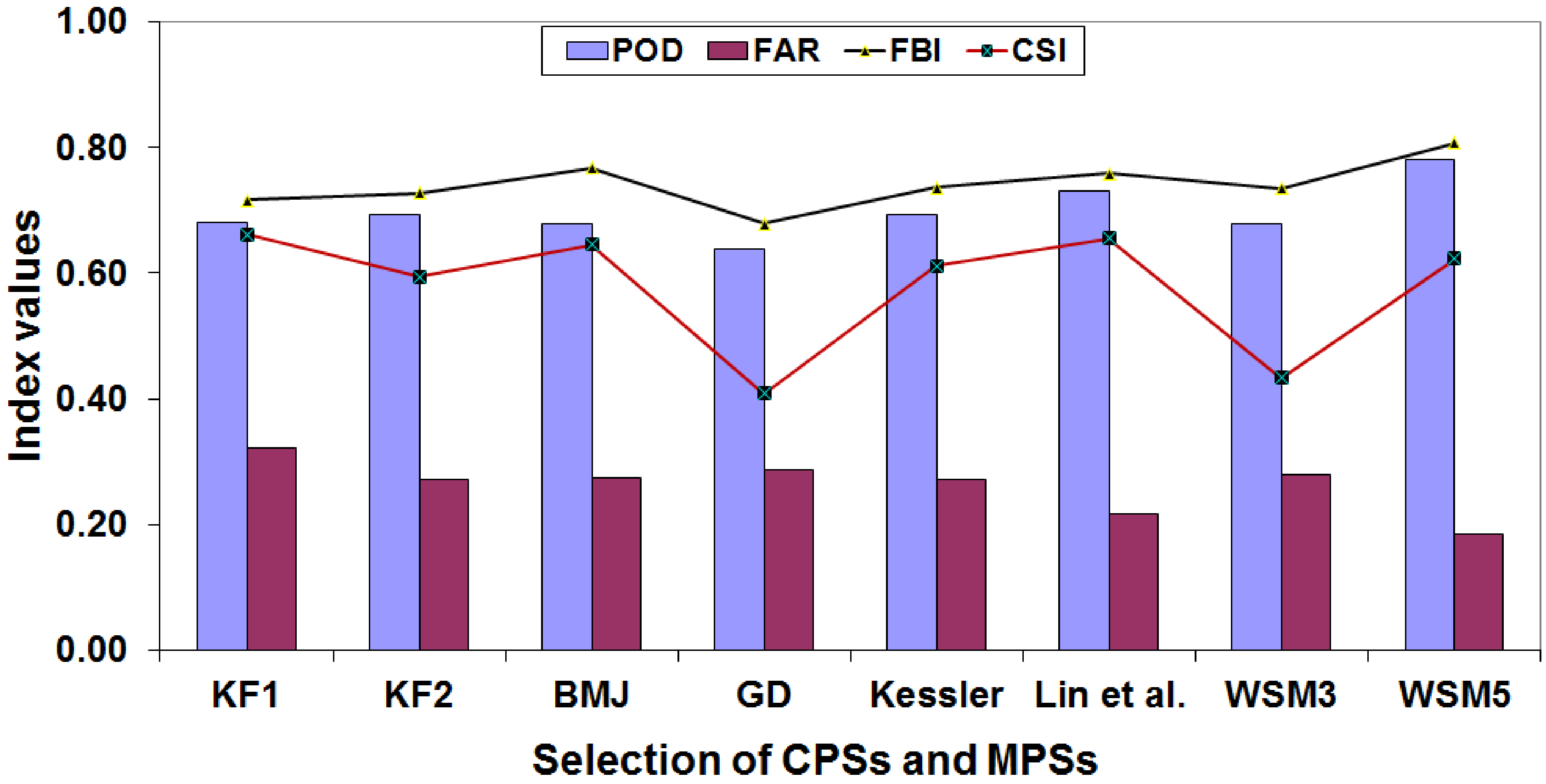

Figure 5: Spatial variation of categorical indices with selection of different CPSs and MPSs during York Flood - 1999

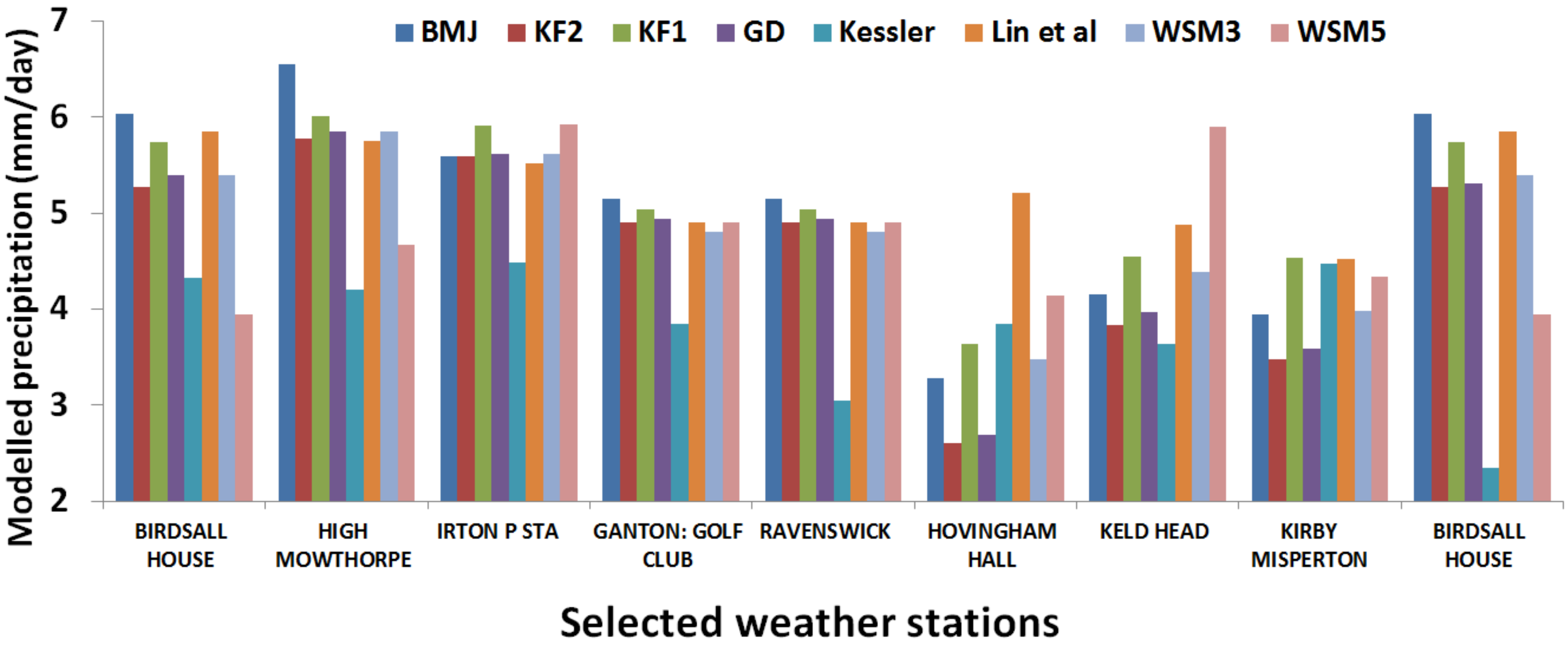

Figure 6: WRF simulated precipitation under different CPSs /MPSs and observed catchment precipitations during 'York Flood -1999' corresponding to different weather stations [daily average of 1st March- 14th March 1999]

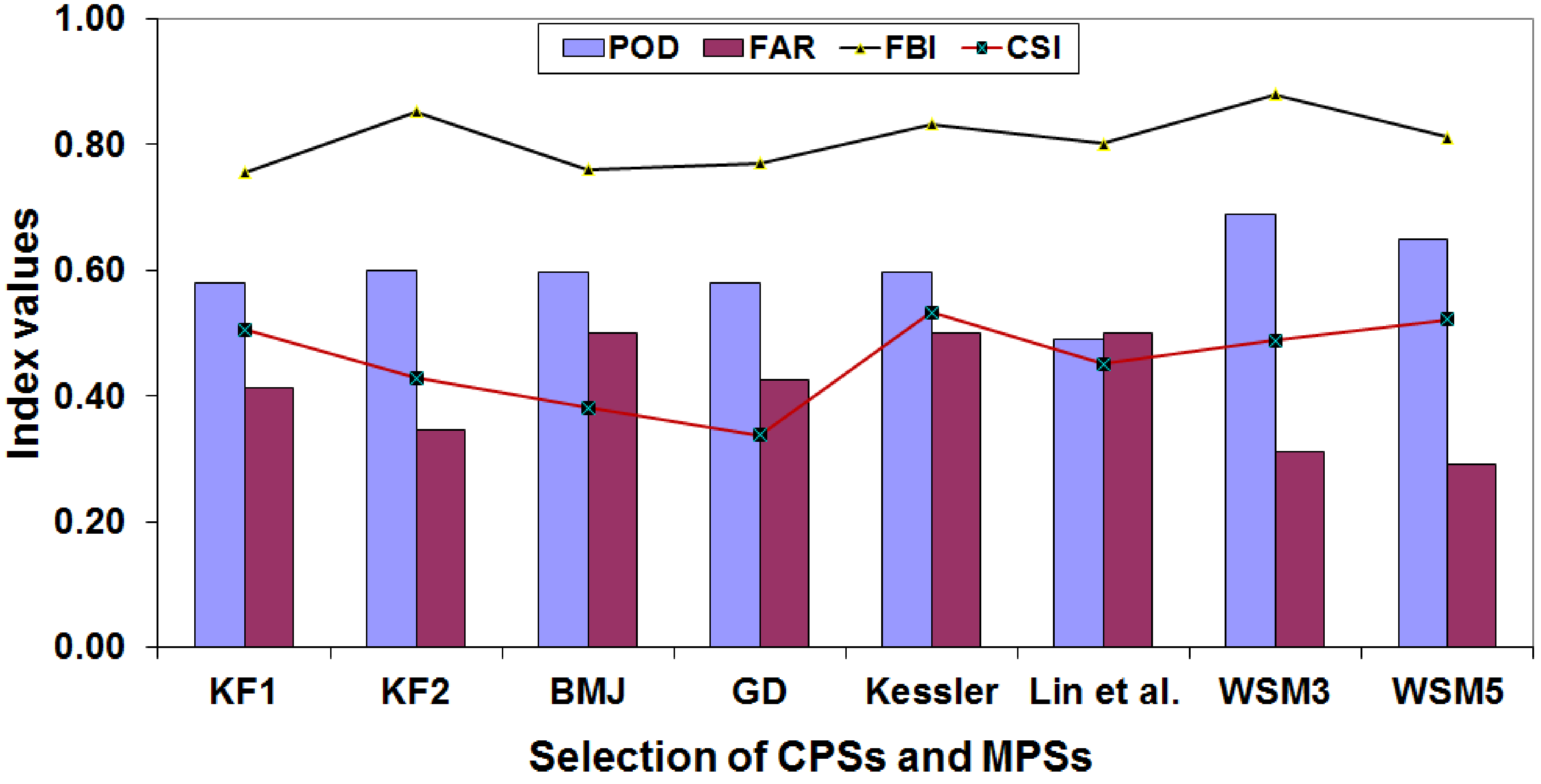

Figure 7: Temporal variation of categorical indices with selection of different CPSs and MPSs during York Flood- 1999

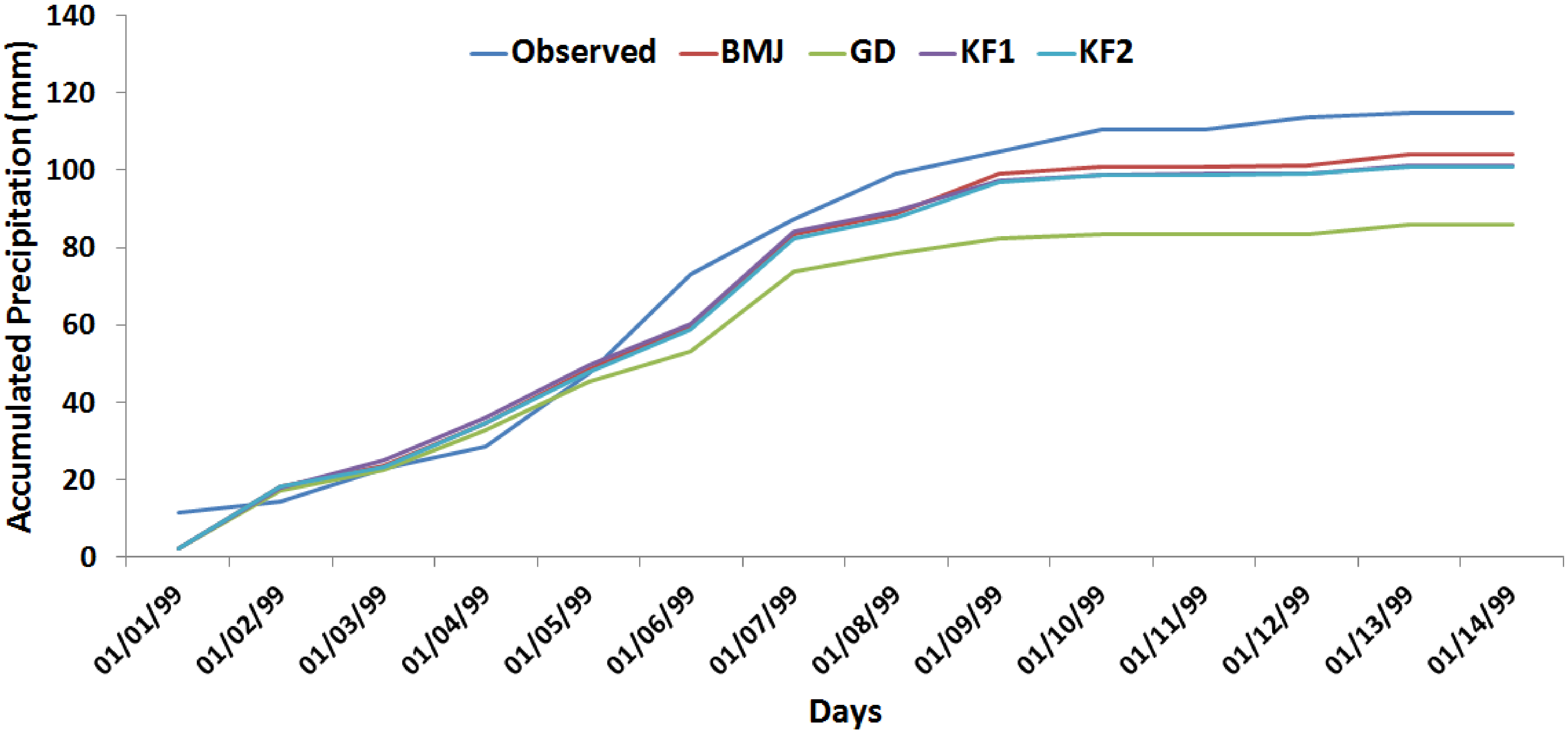

Figure 8: Cumulative variation of WRF predicted precipitation during 'York Flood – 1999' using different CPSs

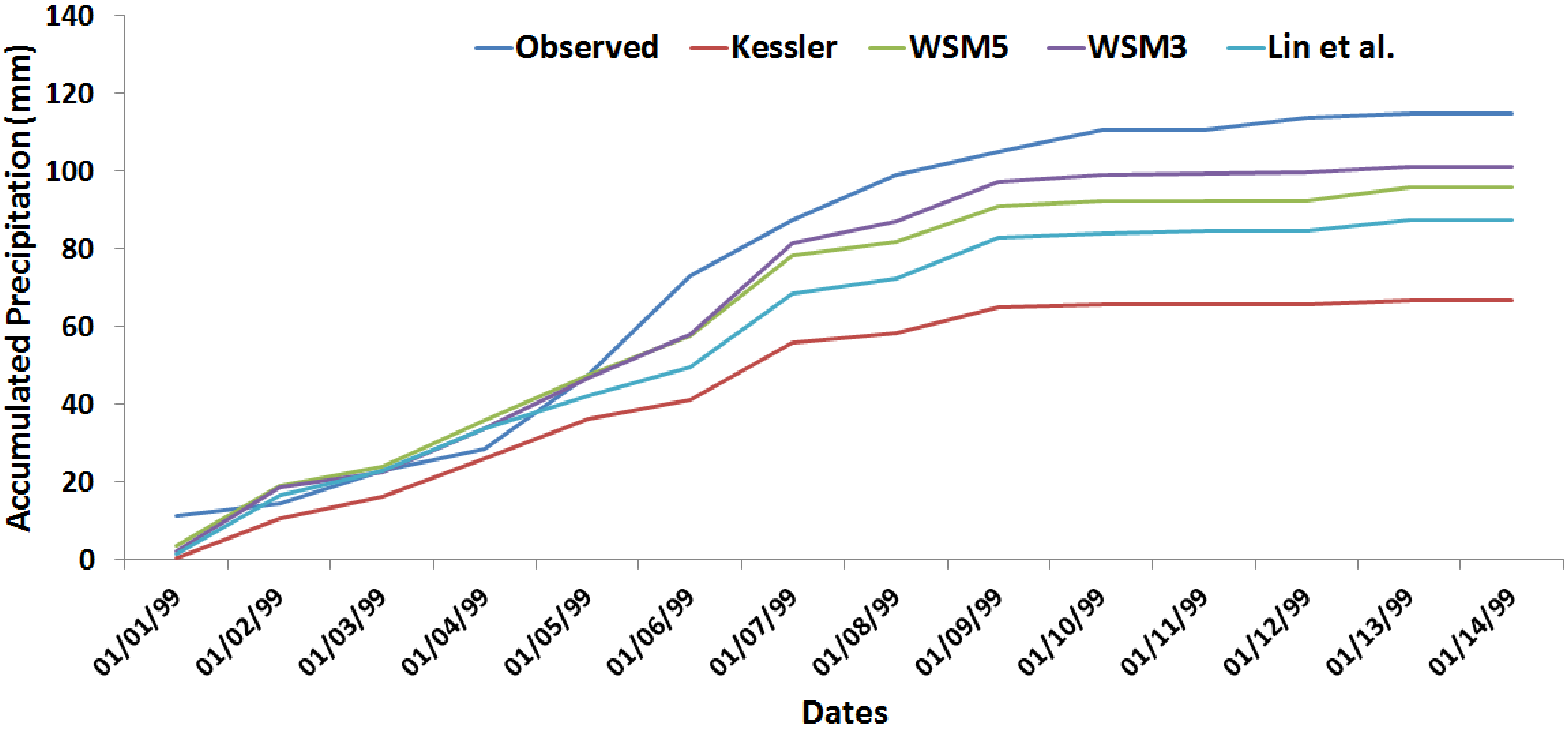

Figure 9: Cumulative variation of WRF predicted precipitation during 'York Flood – 1999' using different MPSs

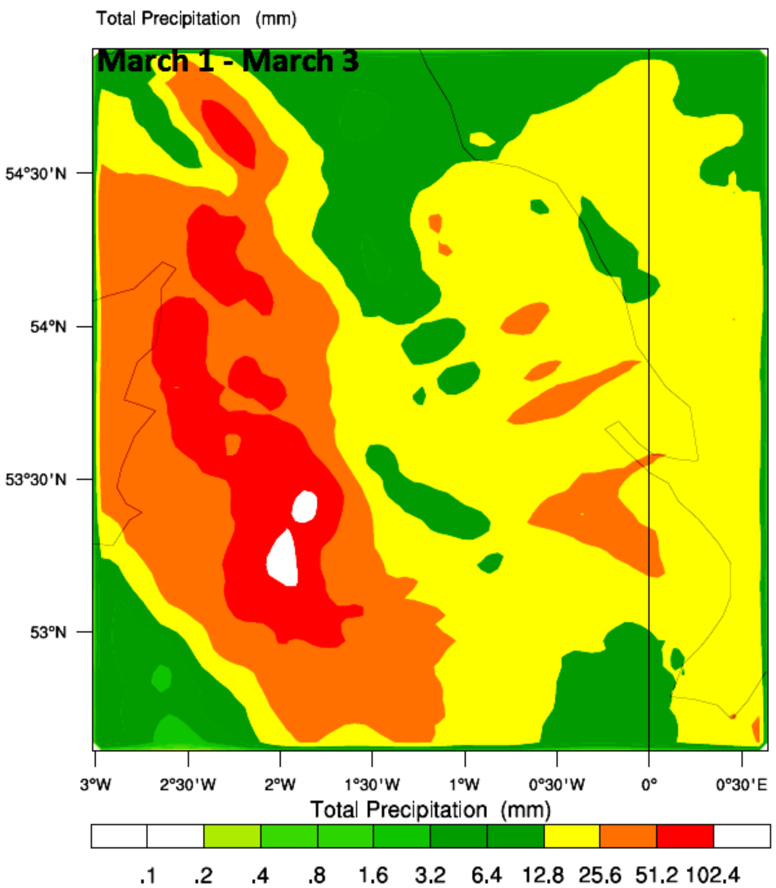
Total Precipitation (mm)
March 1 - March 3
54°30'N
54°N
53°30'N
53°N
3°W
2°30'W
2°W
1°30'W
1°W
0°30'W
0°
0°30'E
Total Precipitation (mm)
.1 .2 .4 .8 1.6 3.2 6.4 12.8 25.6 51.2 102.4

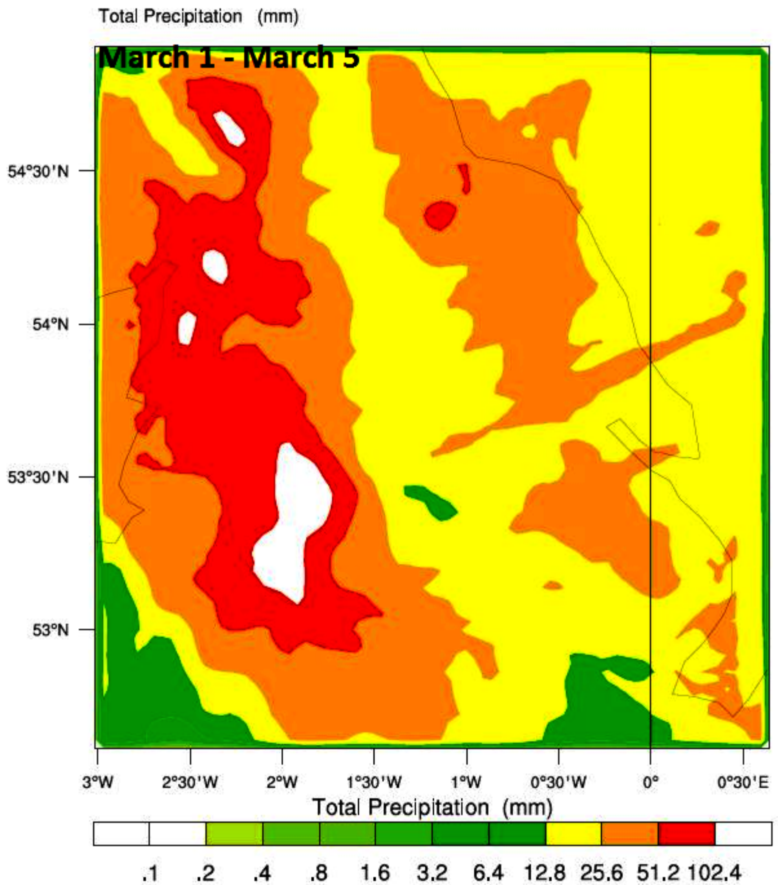
Total Precipitation (mm)
March 1 - March 5
54°30'N
54°N
53°30'N
53°N
3°W
2°30'W
2°W
1°30'W
1°W
0°30'W
0°
0°30'E
Total Precipitation (mm)
.1 .2 .4 .8 1.6 3.2 6.4 12.8 25.6 51.2 102.4

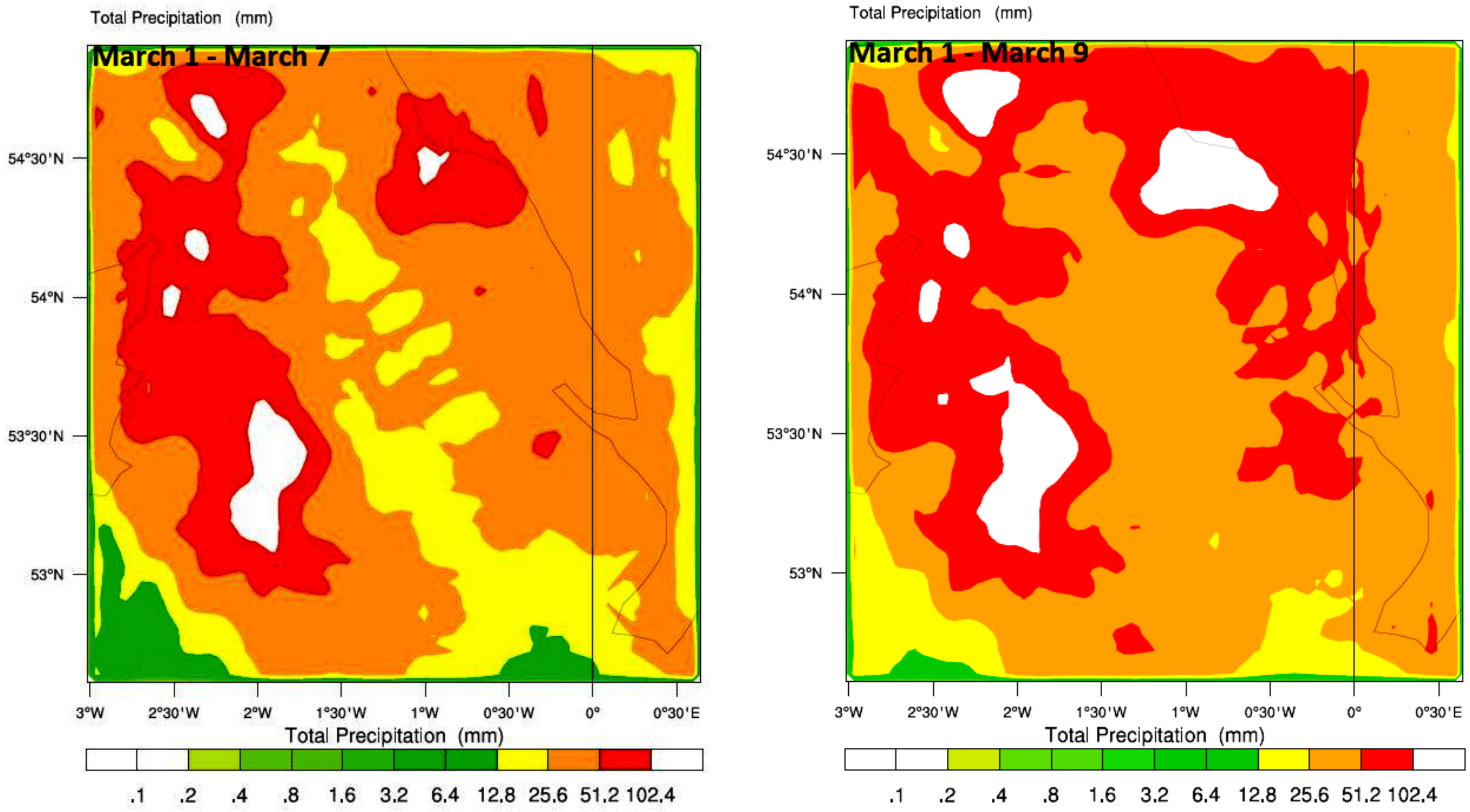

Total Precipitation (mm)
March 1 - March 7
54°30'N
54°N
53°30'N
53°N
3°W
2°30'W
2°W
1°30'W
1°W
0°30'W
0°
0°30'E
Total Precipitation (mm)
.1 .2 .4 .8 1.6 3.2 6.4 12.8 25.6 51.2 102.4
Total Precipitation (mm)
March 1 - March 9
54°30'N
54°N
53°30'N
53°N
3°W
2°30'W
2°W
1°30'W
1°W
0°30'W
0°
0°30'E
Total Precipitation (mm)
.1 .2 .4 .8 1.6 3.2 6.4 12.8 25.6 51.2 102.4

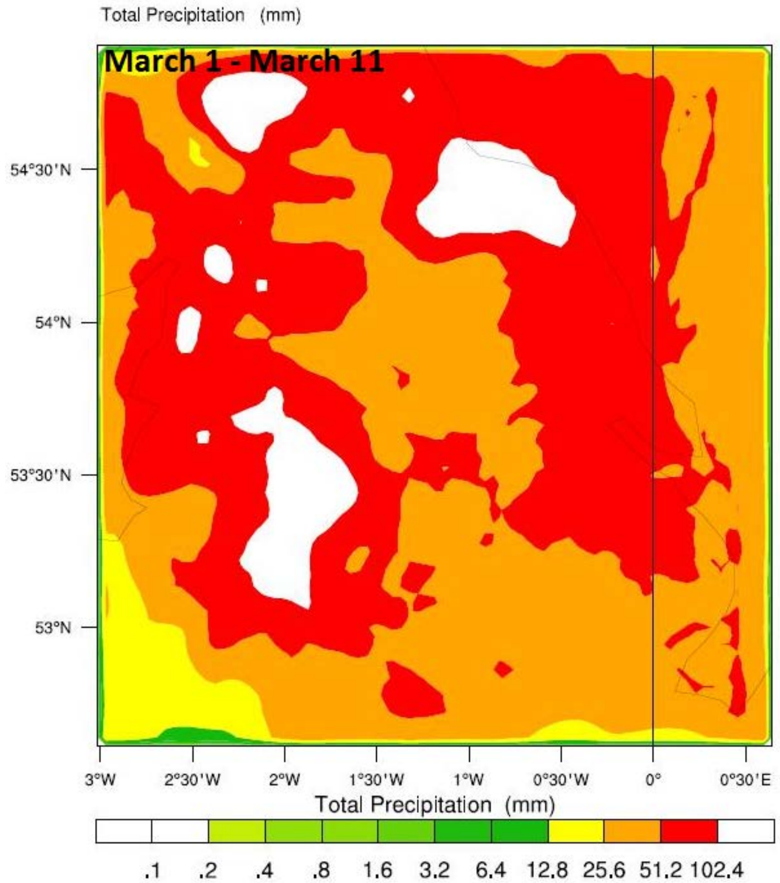
Total Precipitation (mm)
March 1 - March 11
54°30'N
54°N
53°30'N
53°N
3°W
2°30'W
2°W
1°30'W
1°W
0°30'W
0°
0°30'E
Total Precipitation (mm)
.1 .2 .4 .8 1.6 3.2 6.4 12.8 25.6 51.2 102.4

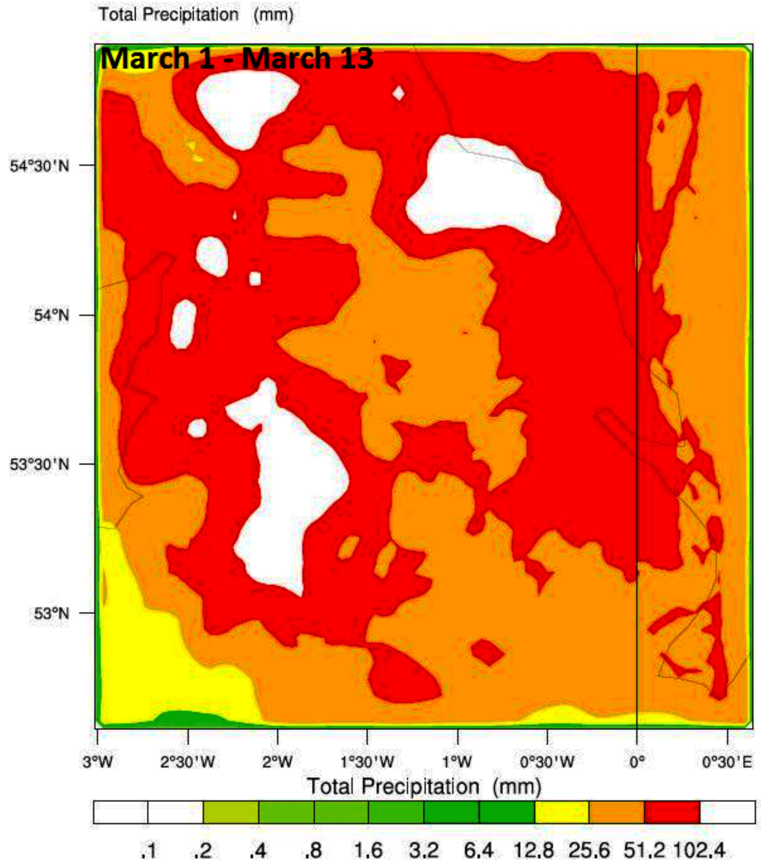
Total Precipitation (mm)
March 1 - March 13
54°30'N
54°N
53°30'N
53°N
3°W
2°30'W
2°W
1°30'W
1°W
0°30'W
0°
0°30'E
Total Precipitation (mm)
.1 .2 .4 .8 1.6 3.2 6.4 12.8 25.6 51.2 102.4

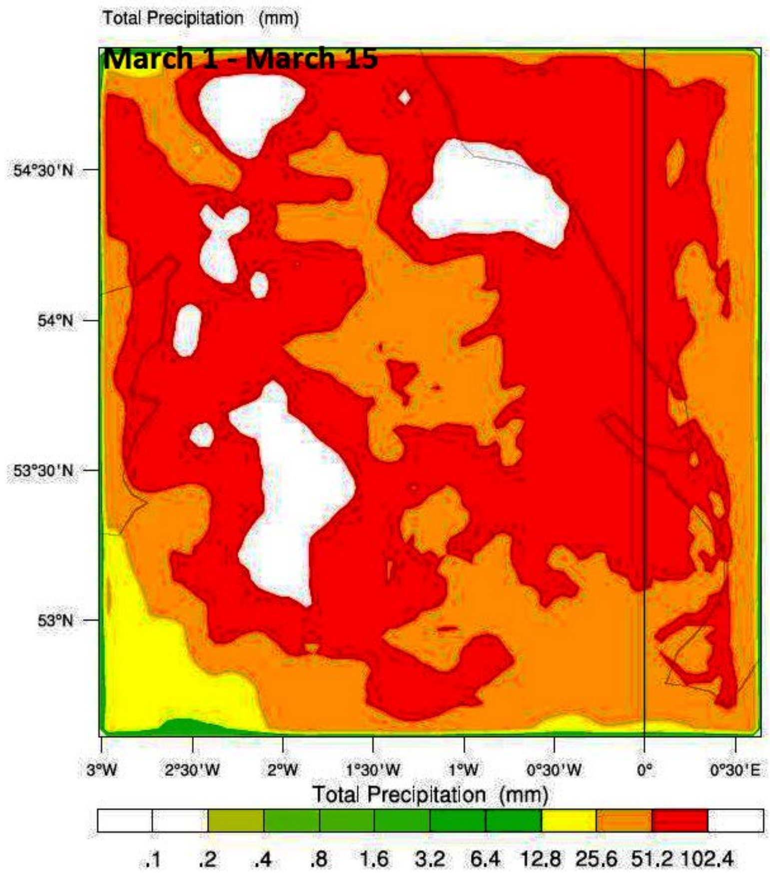

Figure 10: The accumulated precipitation results obtained from WRF with WRF SM3 and BMJ schemes from 1st March to 14th march 1999